Cell Reports
Medicine

Article

An Agonistic Anti-CD137 Antibody Disrupts Lymphoid Follicle Structure and T-Cell-Dependent Antibody Responses

Graphical Abstract

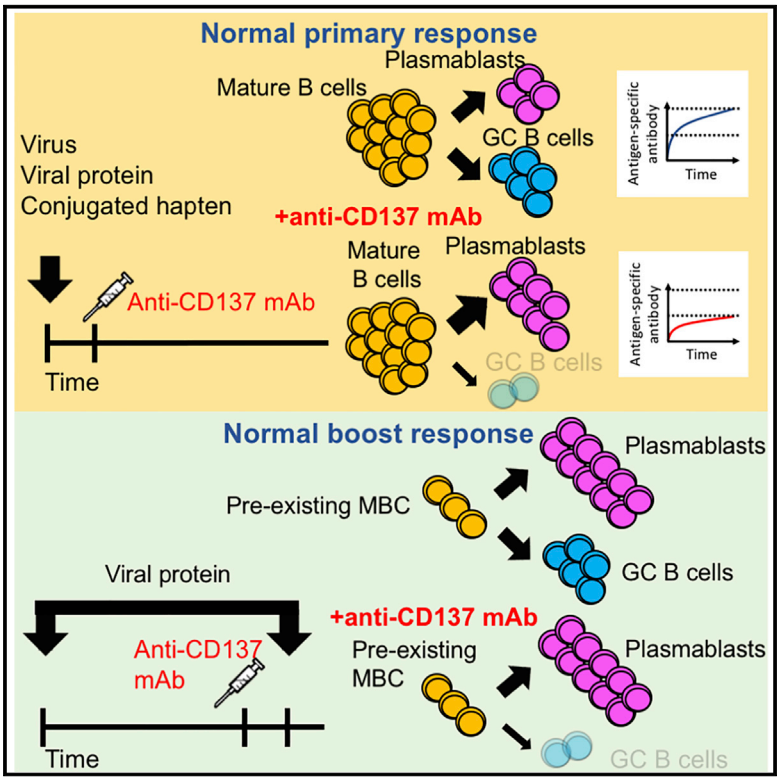

Highlights

- Anti-CD137 antibody impairs B cell responses during chikungunya virus infection
- Anti-CD137 antibody impairs T-cell-dependent antibody responses to subunit vaccines
- Anti-CD137 antibody alters lymphoid follicle structure during virus infection
- Enhanced CD137 signaling in T cells results in defects in germinal B cell responses

Authors

Jun P. Hong, Glennys V. Reynoso, Prabhakar S. Andhey, ..., Maxim Artyomov, Heather D. Hickman, Michael S. Diamond

Correspondence

diamond@wusm.wustl.edu

In Brief

Agonistic anti-CD137 antibodies are being tested in clinical trials for their ability to enhance anticancer immunity. Hong et al. demonstrate that agonistic anti-CD137 antibody treatment causes defects in acute germinal B cell responses after virus infection or T-cell-dependent vaccines that impact long-lasting humoral immunity.

Hong et al., 2020, Cell Reports Medicine *1*, 100035
June 23, 2020
https://doi.org/10.1016/j.xcrm.2020.100035

CellPress

Cell Reports Medicine

CellPress
OPEN ACCESS

Article

An Agonistic Anti-CD137 Antibody Disrupts Lymphoid Follicle Structure and T-Cell-Dependent Antibody Responses

Jun P. Hong,[1] Glennys V. Reynoso,[5] Prabhakar S. Andhey,[2] Amanda Swain,[2] Jackson S. Turner,[2] Adrianus C.M. Boon,[1] Florian Krammer,[8] Ali H. Ellebedy,[2,4] Fabio Zanini,[6,7] Maxim Artyomov,[2,4] Heather D. Hickman,[5] and Michael S. Diamond[1,2,3,4,9,*]

[1]Department of Medicine, Washington University School of Medicine, St. Louis, MO 63110, USA
[2]Department of Pathology and Immunology, Washington University School of Medicine, St. Louis, MO 63110, USA
[3]Department of Molecular Microbiology, Washington University School of Medicine, St. Louis, MO 63110, USA
[4]Center for Human Immunology and Immunotherapy Programs, Washington University School of Medicine, St. Louis, MO 63110, USA
[5]Viral Immunity and Pathogenesis Unit, Laboratory of Clinical Immunology and Microbiology, National Institute of Allergy and Infectious Diseases, National Institutes of Health, Bethesda, MD 20892, USA
[6]Department of Bioengineering, Stanford University, Stanford, CA 94305, USA
[7]Prince of Wales Clinical School, Lowy Cancer Research Centre, University of New South Wales, Sydney, NSW, Australia
[8]Department of Microbiology, Icahn School of Medicine at Mount Sinai, New York, NY 10029, USA
[9]Lead Contact
*Correspondence: diamond@wusm.wustl.edu
https://doi.org/10.1016/j.xcrm.2020.100035

SUMMARY

CD137 is a costimulatory receptor expressed on natural killer cells, T cells, and subsets of dendritic cells. An agonistic monoclonal antibody (mAb) against CD137 has been used to reduce tumor burden or reverse autoimmunity in animal models and clinical trials. Here, we show that mice treated with an agonistic anti-CD137 mAb have reduced numbers of germinal center (GC) B cells and follicular dendritic cells (FDCs) in lymphoid tissues, which impair antibody responses to multiple T-cell-dependent antigens, including infectious virus, viral proteins, and conjugated haptens. These effects are not due to enhanced apoptosis or impaired proliferation of B cells but instead correlate with changes in lymphoid follicle structure and GC B cell dispersal and are mediated by CD137 signaling in $CD4^+$ and $CD8^+$ T cells. Our experiments in mice suggest that agonistic anti-CD137 mAbs used in cancer and autoimmunity therapy may impair long-term antibody and B cell memory responses.

INTRODUCTION

Agonistic monoclonal antibodies (mAbs) targeting the costimulatory receptor CD137 enhance antibody-dependent cell-mediated cytotoxicity by natural killer (NK) cells and proliferation, functional activity, and survival of T cells.[1] Based on these functions and other pre-clinical studies,[1–6] anti-CD137 mAbs have been combined with chemotherapy and immunotherapy in human cancer clinical trials.[1] Anti-CD137 mAbs also have been evaluated in autoimmune disease models based on their ability to induce tolerogenic dendritic cells (DCs) and regulatory T cells (Tregs).[7,8] Although early-stage clinical trials have shown promising antitumor effects, dose-dependent liver toxicity of anti-CD137 mAb has been reported.[9] Moreover, it remains unclear whether anti-CD137-based drugs could have additional effects of immune activation, which could impact their widespread use.

Germinal centers (GCs) in lymphoid tissues are complex anatomical sites where somatic hypermutation and antibody isotype switching in B cells occurs. GC B cells proliferate extensively and traffic through the light and dark zones as part of an antigen-driven affinity-based clonal selection and expansion process (reviewed in Mesin et al.[10]). In the light zone, GC B cells recognize antigens on follicular DCs (FDCs) and undergo selection after antigen internalization, processing, and presentation. GC B cells interact with cognate follicular helper T (Tfh) cells, which themselves are instructed by follicular regulatory T (Tfr) cells.[11] Although some GC B cells that express B cell receptors (BCRs) with a higher affinity for antigens receive T cell help, re-enter the dark zone, selectively expand, and undergo somatic hypermutation, lower affinity GC B cells without T cell help often apoptose.[12] The GC reaction culminates in the generation of high-affinity memory B cells (MBCs) and terminally differentiated long-lived plasma cells (LLPCs), the latter of which durably secrete antibody.

Previously, while evaluating anti-CD137 mAb as a possible therapy for chronic virus infection in mice, we unexpectedly observed reduced numbers of GC B cells.[13] Here, we evaluated the consequences of agonistic anti-CD137 mAb treatment on antibody and B cell responses in the context of immunization

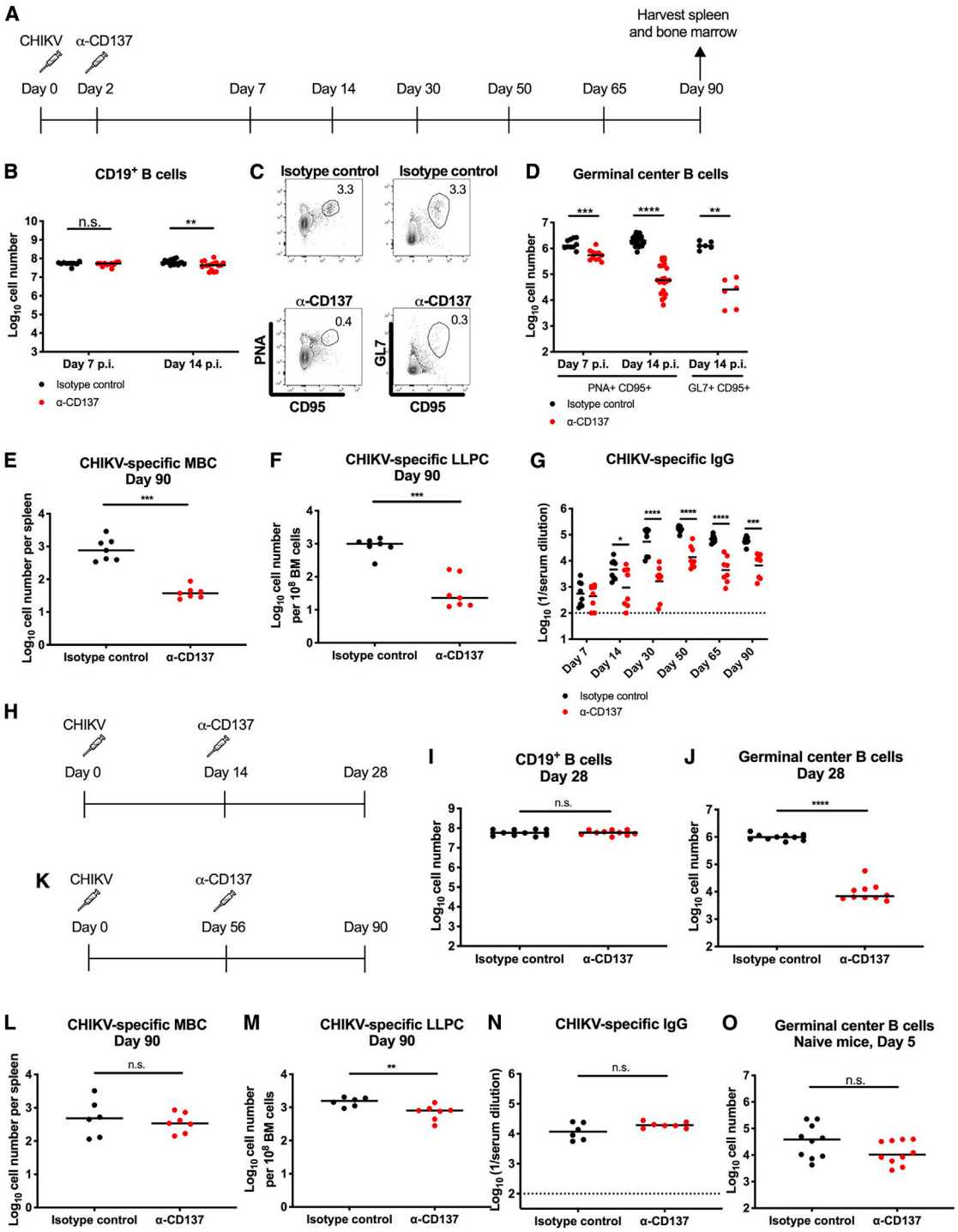

Figure 1. Anti-CD137 mAb Treatment Reduces the Number of GC B Cells, Antigen-Specific MBCs, and LLPCs when Given before GC Formation

(A–G) Four-week-old WT C57BL/6 male mice were inoculated with 10^3 focus-forming units (FFU) of CHIKV (A). At 2 dpi, 400 μg of agonistic anti-CD137 or isotype control mAb was administered by an i.p. route. The numbers of total $CD19^+$ B cells (B) and PNA^+CD95^+ or $GL7^+CD95^+$ GC B cells (C and D) in the spleen at 7 and 14 dpi were analyzed by flow cytometry. (C) Representative dot plots of GC B cells are shown. At day 90 dpi, spleen and bone marrow were harvested to assess antigen-specific MBCs (E) and LLPCs (F). (G) Serum was harvested at 7, 14, 30, 50, 65, and 90 dpi, and anti-CHIKV IgG titers were measured.

(H–J) Four-week-old WT C57BL/6 male mice were inoculated with 10^3 FFU of CHIKV (H). At 14 dpi, 400 μg of agonistic anti-CD137 or isotype control mAb was administered by an i.p. route. The numbers of total $CD19^+$ B cells (I) and PNA^+CD95^+ GC B cells (J) in the spleen at 28 dpi were analyzed by flow cytometry.

(legend continued on next page)

or virus infection in mice. During infection with chikungunya virus (CHIKV), an emerging alphavirus, anti-CD137 mAb treatment resulted in reduced numbers of GC B cells, MBCs, and LLPCs. Administration of agonistic anti-CD137 mAb also dampened the serum antibody response in mice immunized with other T-cell-dependent antigens (influenza virus hemagglutinin [HA] and 4-hydroxy-3-nitrophenylacetyl hapten [NP]-conjugated keyhole limpet hemocyanin [KLH]) but not with a T-cell-independent antigen (NP-Ficoll) or at homeostasis. The reduction of GC B cell numbers caused by anti-CD137 mAb was associated with altered GC architecture; attrition of FDCs, which are critical for GC formation and maintenance; and dispersal of GC B cells. Inhibition of GC formation by anti-CD137 mAb required cell-intrinsic signaling of T cells. Thus, in mice, anti-CD137 mAb treatment results in the activation of T cells that impairs GC development and MBC formation and inhibits the induction of long-lived antigen-specific antibody responses.

RESULTS

Anti-CD137 mAb Treatment Diminishes GCs and Antigen-Specific MBCs and LLPCs

Because we previously observed diminished GC numbers in CHIKV-infected mice treated with anti-CD137 mAb,[13] we evaluated the effect on long-term MBC responses. Four-week-old C57BL/6 male mice were inoculated subcutaneously (s.c.) in the foot with CHIKV (day 0) and then injected by an intraperitoneal (i.p.) route with anti-CD137 mAb at 2 days postinfection (dpi) (Figure 1A). At 14 dpi, mice treated with anti-CD137 mAb had slightly reduced numbers of $CD19^+$ B cells in the spleen compared to isotype control mAb-treated animals (1.4-fold, $p < 0.01$; Figure 1B). However, the number of GC B cells (as determined by either peanut agglutinin lectin $[PNA]^+CD95^+$ or $GL7^+CD95^+$ staining) in the spleen at 14 dpi was reduced to a greater extent (33.3- to 43.3-fold, $p \leq 0.0001$; Figures 1C and 1D). To assess the long-term consequence on the humoral response, serum was obtained at 7, 14, 30, 50, 65, and 90 dpi, and the spleen and bone marrow were harvested at 90 dpi to profile antigen-specific MBCs and LLPCs (Figure 1A). Anti-CD137 mAb-treated mice had lower numbers of CHIKV-specific MBCs in the spleen (20.6-fold, $p < 0.001$) and LLPCs in the bone marrow (43.5-fold, $p < 0.001$) than isotype control mAb-treated animals (Figures 1E and 1F). Serum anti-CHIKV immunoglobulin G (IgG) levels also were reduced in anti-CD137 mAb-treated mice compared to isotype control mAb-treated animals beginning at 14 dpi (4.9- to 33.1-fold, $p \leq 0.0001$; Figure 1G).

To test the effect of anti-CD137 mAb on a later stage of the GC reaction, we treated CHIKV-infected mice with anti-CD137 mAb at 14 dpi and analyzed cell numbers at 28 dpi (Figure 1H). Although the number of total $CD19^+$ B cells did not change (Figure 1I), the number of PNA^+CD95^+ GC B cells in anti-CD137 mAb-treated mice was decreased (142-fold, $p \leq 0.0001$) compared to isotype control mAb-treated animals (Figure 1J). We then evaluated the effect of anti-CD137 mAb on an established MBC response. CHIKV-infected mice were treated with anti-CD137 mAb at 56 dpi, a time when the GC reaction is fully established,[10,14] and spleen and bone marrow were harvested at 90 dpi for analysis (Figure 1K). Anti-CD137 mAb-treated mice showed similar numbers of CHIKV-specific MBCs and only slightly reduced numbers (2-fold, $p < 0.01$) of CHIKV-specific LLPCs compared to isotype control mAb-treated animals (Figures 1L and 1M). Correspondingly, serum anti-CHIKV IgG levels at 90 dpi were similar between mice treated at 56 dpi with anti-CD137 or isotype control mAb (Figure 1N). These data suggest that anti-CD137 mAb treatment inhibits the development of MBCs and LLPCs but has a minimal effect on the maintenance of established MBC compartments. In naive pathogen-free mice, anti-CD137 mAb treatment did not substantially alter the relatively low number of GC B cells seen at homeostasis (Figure 1O).

Anti-CD137 mAb Treatment Reduces T-Cell-Dependent but Not -Independent Antibody Responses

We evaluated the effect of anti-CD137 mAb treatment after immunization with model T-cell-dependent (NP-KLH) and T-cell-independent (NP-Ficoll) antigens.[15] Four-week-old C57BL/6 male mice were immunized by the i.p. route with NP-KLH or NP-Ficoll and then treated with anti-CD137 mAb 2 days later. Sera were obtained at multiple time points postimmunization, and at the last time point, bone marrow was harvested to profile LLPCs (Figures 2A and 2F). Spleens from a separate cohort of mice were harvested at 30 days postimmunization to quantify MBCs. Anti-CD137 mAb treatment reduced the number of GC B cells (18-fold, $p < 0.01$) and NP-specific IgG^+ MBCs (7-fold, $p < 0.001$) at 14 and 30 days postimmunization, respectively, in mice administered NP-KLH (Figures 2B and 2C). The number of NP-specific LLPCs (12-fold, $p < 0.0001$) also was reduced at 130 days postimmunization (Figure 2D). Correspondingly, serum anti-NP IgG levels were diminished in anti-CD137 mAb-treated mice beginning at 28 days postimmunization (Figure 2E). In NP-Ficoll-immunized mice, the numbers of NP-specific IgM^+ plasmablasts at days 3 and 7, NP-specific IgM^+ MBCs at day 30, and IgG^+ LLPCs at day 130 were equivalent between anti-CD137 and isotype control mAb-treated groups (Figures 2G–2I). Consistent with these data, serum anti-NP IgM and IgG levels generally were similar whether animals received anti-CD137 or not (Figures 2J and 2K). Thus, anti-CD137 treatment affects B cell responses that require T-cell-dependent help.

(K–N) Four-week-old WT C57BL/6 male mice were inoculated with 10^3 FFU of CHIKV (K). At 56 dpi, 400 μg of agonistic anti-CD137 or isotype control mAb was administered by an i.p. route. At 90 dpi, spleen and bone marrow were harvested to assess antigen-specific MBCs (L) and LLPCs (M). At this time, anti-CHIKV IgG titers (N) also were measured.

(O) Four-week-old naive WT C57BL/6 male mice were administered with 400 μg of agonistic anti-CD137 or isotype control mAb by an i.p. route. The numbers of PNA^+CD95^+ GC B cells in the spleen at 5 days after treatment were analyzed by flow cytometry. Symbols represent individual mice, bars indicate median values, and dotted lines denote the limit of detection of the assay. Data are pooled from 2 to 4 independent experiments (Mann-Whitney test, except for serum antibody titers where two-way ANOVA with Sidak post-test was used: *$p < 0.05$; **$p < 0.01$; ***$p < 0.001$; ****$p < 0.0001$; n.s., not significant).

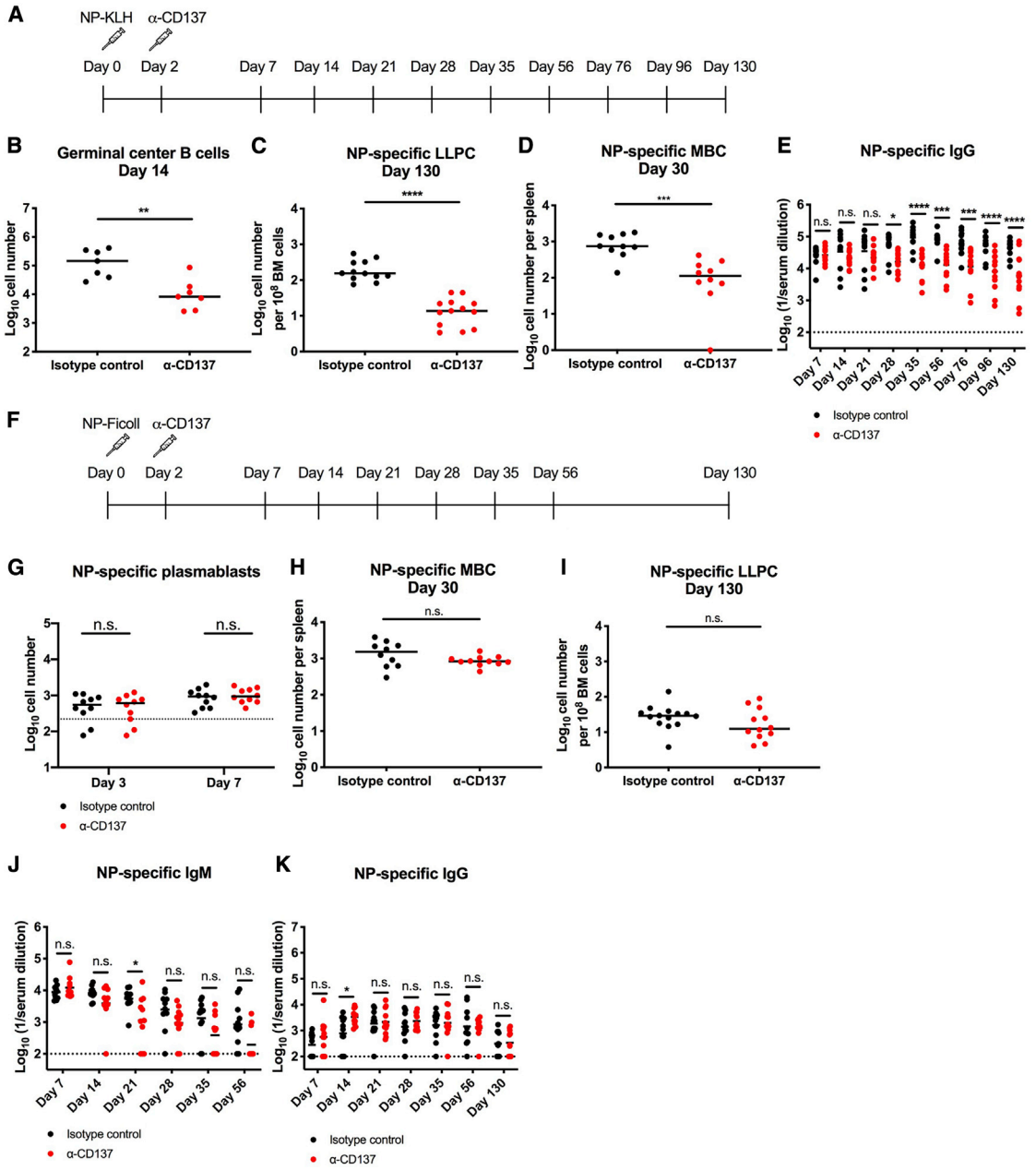

Figure 2. Anti-CD137 mAb Treatment Dampens T-Cell-Dependent Antibody Responses

(A–F) Four-week-old C57BL/6 male mice were injected by i.p. route with 5 μg of NP-KLH (A) or 10 μg of NP-Ficoll (F). At 2 dpi, 400 μg of agonistic anti-CD137 or isotype control mAb was administered by an i.p. route. (B–E) After immunization with NP-KLH, the number of PNA^+CD95^+ GC B cells (B) in the spleen at 14 days postimmunization was analyzed by flow cytometry. At 30 days postimmunization, antigen-specific MBCs were harvested from a separate set of animals and profiled (C). At day 130, bone marrow was harvested to profile antigen-specific LLPCs (D). Serum was collected at 7, 14, 21, 28, 35, 56, 76, 96, and 130 days postimmunization, and anti-NP IgG (E) was measured.

(G–K) After immunization with NP-Ficoll, spleens were harvested at day 3 and 7 to assess antigen-specific IgM^+ plasmablasts (G). At 30 days postimmunization, antigen-specific IgM^+ MBCs were harvested and profiled (H). Bone marrow was harvested at day 130 to assess antigen-specific IgG^+ LLPCs (I). Serum was collected at 7, 14, 21, 28, 35, 56, and 130 days postimmunization, and anti-NP IgM (J) and IgG (K) were measured. Symbols represent individual mice, and bars indicate median values, except for serum antibody titers where bars indicate mean values. The IgM and IgG ELISA binding data were analyzed by subtracting the optical density (OD) of naive serum from the OD of serum from immunized animals. Dotted lines represent the baseline number of plasmablasts that secrete NP-binding natural IgM in naive control mice (G) or limit of detection (E, J, and K). Data are pooled from 3 independent experiments (Mann-Whitney test, except for serum antibody titers where two-way ANOVA with Sidak post-test was used: *$p < 0.05$; **$p < 0.01$; ***$p < 0.001$; ****$p < 0.0001$; n.s., not significant).

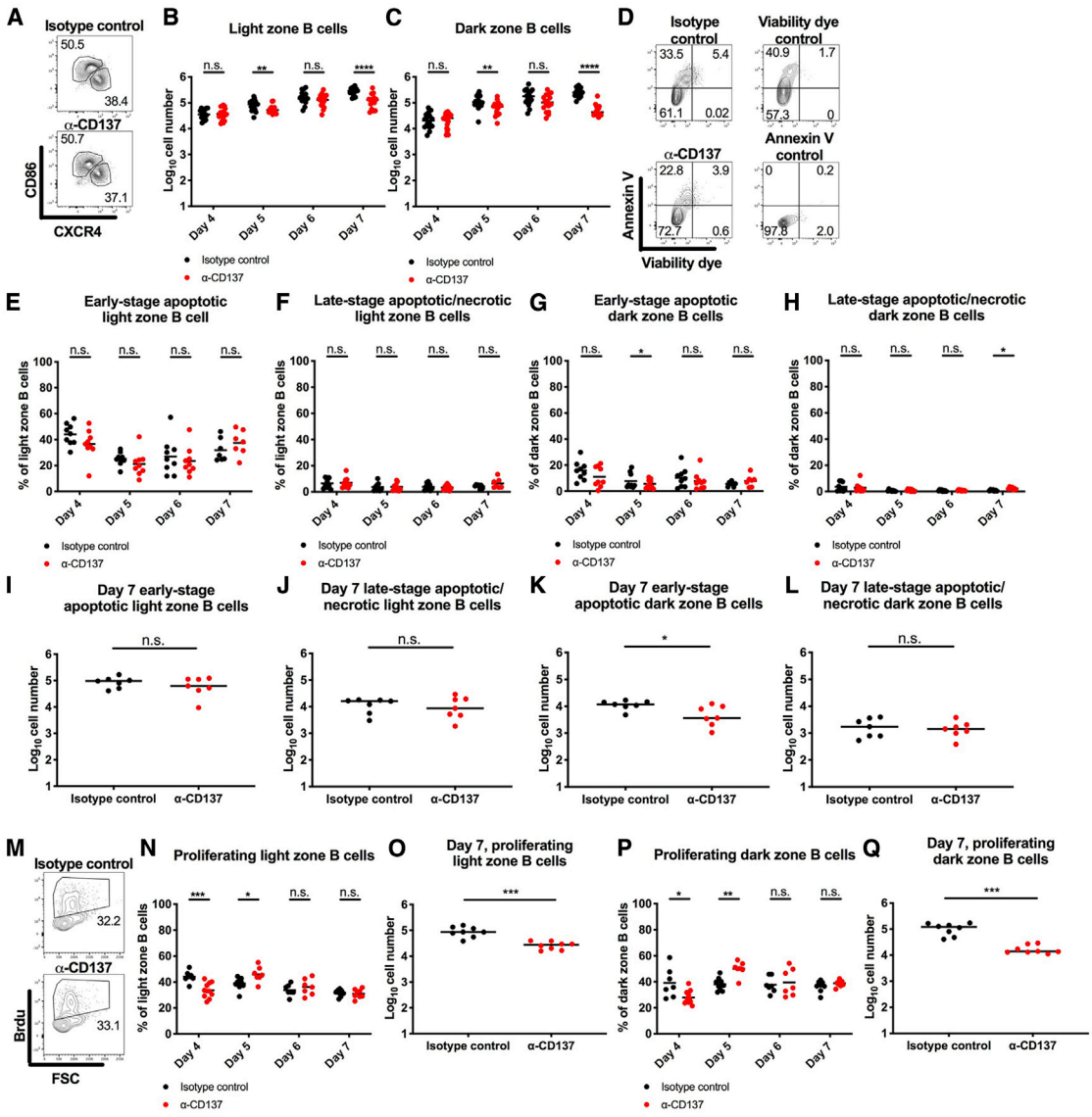

Figure 3. Anti-CD137 mAb Treatment Has a Minimal Effect on Apoptosis and Proliferation of GC B Cells

Four-week-old WT C57BL/6 male mice were inoculated with 10^3 FFU of CHIKV. At 2 dpi, 400 μg of agonistic anti-CD137 or isotype control mAb was administered by an i.p. route. The number of CD86^{hi}CXCR4^{low} light zone B cells (A and B) and CD86^{low}CXCR4^{hi} dark zone B cells (A and C); and the percentage of annexin V$^+$ Viability dye$^-$ early-stage apoptotic light zone (D and E) and dark zone B cells (G), annexin V$^+$ Viability dye$^+$ late-stage apoptotic light (D and F) and dark zone B cells (H), and Brdu$^+$ proliferating light (M and N) and dark zone B cells (P) in the spleen at 4, 5, 6, and 7 dpi were analyzed by flow cytometry. Representative dot plots of light and dark zone B cells (A), apoptotic light zone B cells (D), and proliferating light zone B cells (M) are shown. The total numbers of apoptotic (I–L) and proliferating GC B cells (O and Q) at 7 dpi are shown. Symbols represent individual mice, and bars indicate median values, except for percentages where bars indicate mean values. Data are pooled from 3 independent experiments (Mann-Whitney test: *$p < 0.05$; **$p < 0.01$; ***$p < 0.001$; ****$p < 0.0001$; n.s., not significant). See also Figure S1.

Apoptosis and Proliferation of GC B Cells Are Minimally Affected by Anti-CD137 mAb Treatment

As reductions in GC B cells associated with anti-CD137 mAb treatment might be due to increased cell death, we stained GC B cells with annexin V, which recognizes phosphatidylserine on the plasma membrane of apoptotic cells. In this experiment, CHIKV-infected mice were treated with anti-CD137 mAb at 2 dpi. The total number of CD86^{hi}CXCR4^{lo} light zone and CD86^{lo}CXCR4^{hi} dark zone B cells were reduced slightly at 5 dpi (1.7-fold, $p < 0.01$; 1.5-fold, $p < 0.01$, respectively) but more so at 7 dpi (2.2-fold, $p < 0.0001$; 5.8-fold, $p < 0.0001$, respectively) in anti-CD137 mAb-treated mice compared to isotype control mAb-treated animals (Figures 3A–3C). However, the percentage of annexin V$^+$ Viability dye$^-$ early-stage apoptotic GC B cells in light or dark zone was similar between anti-CD137 and isotype control mAb-treated animals (Figures 3D,

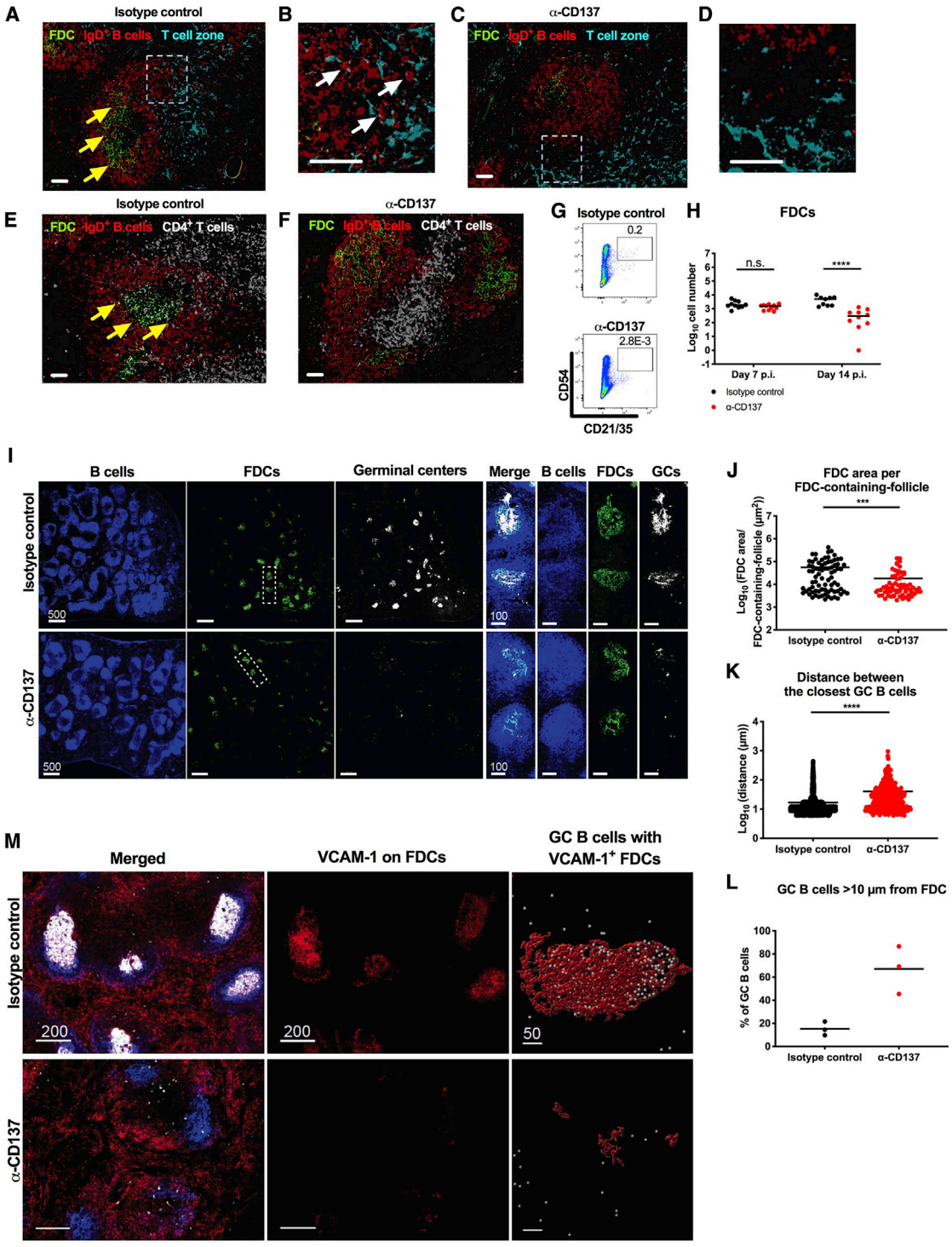

Figure 4. Anti-CD137 mAb Results in Disorganization of B Cell Follicle Architecture in the Spleen

Four-week-old WT C57BL/6 male mice were inoculated with 10^3 FFU of CHIKV. At 2 dpi, 400 μg of agonistic anti-CD137 or isotype control mAb was administered by an i.p. route. Spleens were harvested at 6 dpi (A–D), 7 dpi (E and F), and 14 dpi (I–M) for imaging. (A–D) FDCs (green) were stained for CD21/35; IgD^+ B cells (red); and T cell zone (turquoise), CCL21. (B and D) Insets of the respective dotted boxes. (E and F) FDCs (green) were stained for CD21/35; IgD^+ B cells (red); and $CD4^+$ T cells (snow). White scale bars indicate 50 μm. Yellow arrows indicate IgD^+ B cells surrounding FDCs, and white arrows indicate IgD^+ B cells at the $CCL21^+$ T cell zone border. (G and H) The number of $CD45^-CD21/35^+CD54^+$ FDCs in the spleen at 7 and 14 dpi was analyzed by flow cytometry. (G) Representative flow cytometry dot plots of FDCs are shown. (I) B cells (blue) were stained for B220; FDCs (green), CD21/35; and GC B cells (snow), GL7. White scale bars indicate

(legend continued on next page)

3E, and 3G). Anti-CD137 mAb treatment also did not alter the percentage of annexin V$^+$ Viability dye$^+$ late-stage apoptotic/necrotic GC B cells in the light or dark zones (Figures 3F and 3H). At 7 dpi, the numbers of early-stage apoptotic GC B cells in the light zone and late-stage apoptotic/necrotic GC B cells in the light and dark zones were similar between anti-CD137 and isotype control mAb-treated animals, although early-stage apoptotic GC B cells in the dark zone were reduced slightly after anti-CD137 mAb treatment (Figures 3I–3L). Overall, anti-CD137 mAb treatment does not appear to cause GC B cell deficits by globally promoting cell death.

To determine the effect of anti-CD137 treatment on GC B cell proliferation, we injected 5-bromo-2′-deoxyuridine (Brdu) into CHIKV-infected mice and measured incorporation by GC B cells. The percentage of Brdu$^+$ proliferating GC B cells was similar between animals treated with anti-CD137 and isotype control mAb except for small differences at 4 and 5 dpi (Figures 3M, 3N, and 3P). However, at 7 dpi, anti-CD137 mAb treatment reduced the overall number of proliferating GC B cells due to the decrease in the total number of cells at this time point (Figures 3O and 3Q). We also assessed whether there was any bias toward reducing the percentage of antigen-specific GC B cells by incubating cells with CHIKV-like particles (CHIK VLPs[16]). The percentage of CHIKV-specific GC B cells was comparable between anti-CD137 mAb-treated and isotype control mAb-treated mice except for small differences at 5 dpi (Figures S1A and S1B).

Anti-CD137 mAb Treatment Alters B Cell Follicle Architecture

To examine whether anti-CD137 mAb affects the anatomic structures of the spleen, we performed immunofluorescence staining at 6 (Figures 4A–4D), 7 (Figures 4E and 4F), and 14 (Figure 4I) dpi. At 6 dpi, in isotype control mAb-treated mice, we observed IgD$^+$ B cells surrounding CD21/35$^+$ FDCs and some IgD$^+$ B cells at the border of the CCL21$^+$ T cell zone (Figures 4A and 4B). However, in anti-CD137 mAb-treated animals, the localization of IgD$^+$ B cells at the T cell zone border was altered (Figures 4C and 4D). At 7 dpi, IgD$^+$ B cells surrounded FDCs in the light zone in isotype control mAb-treated mice (Figure 4E), whereas in anti-CD137 mAb-treated animals, IgD$^+$ B cells covered the FDC area (Figure 4F).

We next determined whether anti-CD137 mAb treatment altered the number of FDCs in the spleen. Flow cytometry analysis revealed that the number of CD45$^-$CD21/35$^+$CD54$^+$ FDCs was comparable at 7 dpi but reduced at 14 dpi in anti-CD137 mAb-treated mice (17-fold, $p < 0.0001$; Figures 4G and 4H). Immunofluorescence microscopy confirmed that at 14 dpi the numbers of FDCs and GC B cells were decreased and/or dispersed in anti-CD137 mAb-treated mice compared to isotype control mAb-treated animals (Figures 4I–4L). In the context of antigen stimulation, FDCs in secondary B cell follicles upregulate the expression of ICAM-1 (CD54) and VCAM-1 (CD106), which support integrin- ($\alpha_L\beta_2$ (CD11a/CD18) and $\alpha_4\beta_1$ (CD49d/CD29))-mediated interactions with GC B cells.[17] As expected, at 14 dpi, in isotype control mAb-treated mice, VCAM-1 was expressed by CD21/35$^+$ FDCs, and this was associated with colocalization of GL7$^+$ GC B cells (Figure 4M). In contrast, CD21/35$^+$ FDCs in anti-CD137 mAb-treated animals did not express VCAM-1 or colocalize with GL7$^+$ GC B cells (Figure 4M).

Loss of GC Formation after Agonistic Anti-CD137 mAb Treatment Requires T-Cell-Intrinsic Signaling

We first evaluated a possible role of CD137 signaling on stromal cells including FDCs, by transplanting wild-type (WT) or CD137$^{-/-}$ bone marrow into irradiated CD137$^{-/-}$ mice (Figure 5A) and confirming reconstitution (Figure 5B). Anti-CD137 mAb treatment reduced the number of GC B cells in mice receiving WT but not CD137$^{-/-}$ bone marrow (Figure 5C). For the reciprocal experiment, T cell receptor (TCR)$\beta\delta^{-/-}$ mice were used as recipients because some T cell subsets (e.g., natural killer T and memory T cells) in WT recipients are radioresistant[18] and we wanted to deplete endogenous T cells completely (Figure 5D). Anti-CD137 mAb treatment reduced the number of GC B cells in TCR$\beta\delta^{-/-}$ mice receiving WT but not CD137$^{-/-}$ bone marrow (Figure 5E). These experiments suggest that CD137-mediated signaling in radiosensitive, hematopoietic cells is required to reduce the number of GC B cells.

T cells are one of the principal immune cell subsets that express CD137 in the spleen of CHIKV-infected mice at 2 dpi.[13] To test whether anti-CD137 mAb treatment reduced the number of GC B cells through CD137 signaling in T cells, we adoptively transferred into recipient TCR$\beta\delta^{-/-}$ mice combinations of CD4$^+$ and CD8$^+$ T cells isolated from WT or CD137$^{-/-}$ mice (Figure 5F). Anti-CD137 mAb treatment reduced the number of GC B cells in mice receiving WT CD4$^+$ T cells + WT CD8$^+$ T cells, CD137$^{-/-}$ CD4$^+$ T cells + WT CD8$^+$ T cells, or WT CD4$^+$ T cells + CD137$^{-/-}$ CD8$^+$ T cells (15.0- to 20.5-fold, $p < 0.001$) but not in mice receiving CD137$^{-/-}$ CD4$^+$ + CD137$^{-/-}$ CD8$^+$ T cells (Figure 5G). Thus, CD137-mediated signaling in either CD4$^+$ or CD8$^+$ T cells is required to inhibit GC B cell production.

Anti-CD137 mAb Treatment Promotes Proinflammatory Signatures in Cycling CD8$^+$ T Cells, Neutrophils, and Differentiating Monocytes

To define global transcriptional changes in lymphoid tissues of mice treated with anti-CD137 mAb, we performed single-cell RNA sequencing (scRNA-seq) on splenocytes harvested from CHIKV-infected mice during the acute phase of infection (3 and 7 dpi). Immune cell subsets were identified by their cell-type-specific gene expression: *CD3e* (T cells), *Ncr1* (NK cells), *CD79a* (B cells), *Flt3* (DCs), *Sdc1* (plasmablasts), *Adgre1* (macrophages), *S100a8* (neutrophils), and *Ccr2/Ly6c2* (monocytes) (Figure S2A).

500 μm or 100 μm (insets). Each symbol represents an individual FDC-containing follicle (J), GC B cell (K), or spleen (L), and bars indicate mean values. Quantification was performed for FDC area per FDC-containing-follicle (J), distance between the closest GC B cells (K), and GC B cells greater than 10 μm from an FDC (L). (M) Left and middle: FDCs (blue) were stained for CD21/35; VCAM-1 (red); merge (white). (M) Right: GC B cells (white) were stained for GL7; VCAM-1$^+$ FDCs (red). White scale bars indicate 200 μm or 50 μm (insets). The images are representative of 3 spleens per group from 2 independent experiments (Mann-Whitney test: ***$p < 0.001$; ****$p < 0.0001$; n.s., not significant).

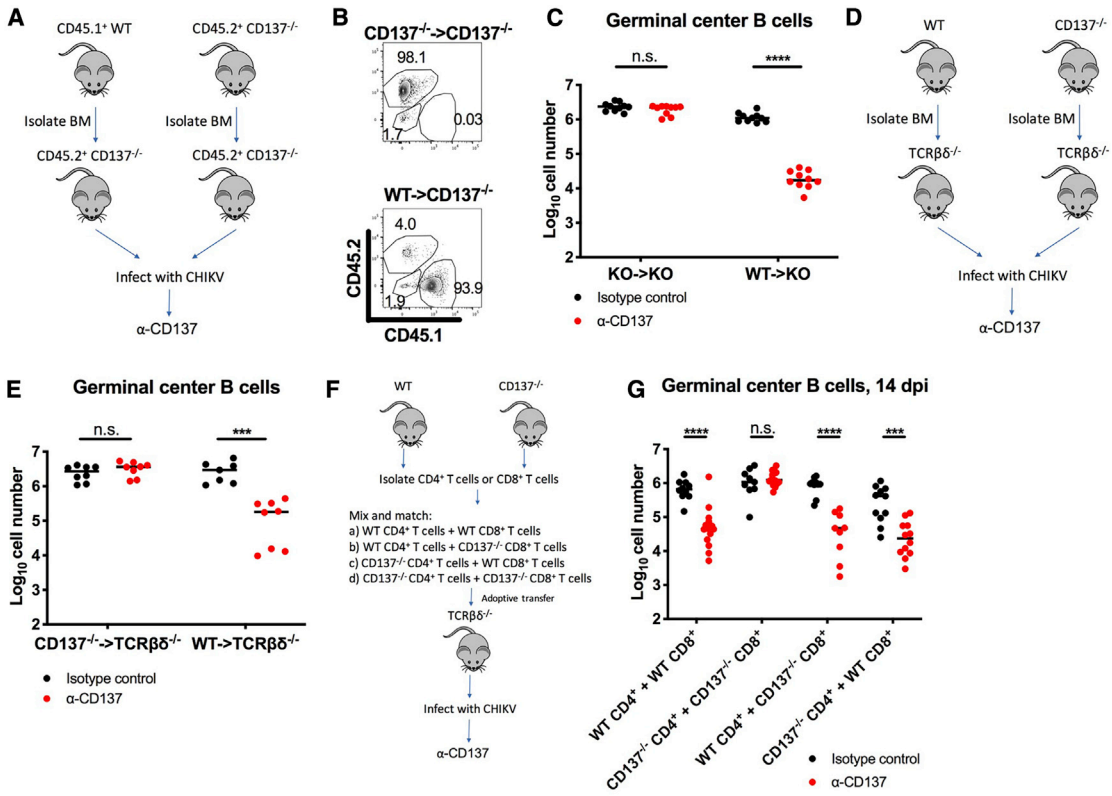

Figure 5. Cell-Intrinsic CD137 Signaling in CD4$^+$ or CD8$^+$ T Cells Is Required for Anti-CD137 mAb-Mediated Inhibition of the GC Reaction

Four-week-old CD137$^{-/-}$ (A) or TCRβδ$^{-/-}$ (D) mice were irradiated and then received bone marrow cells from WT or CD137$^{-/-}$ mice. After 8 weeks, recipient mice were inoculated with 10^3 FFU of CHIKV. At 2 dpi, 400 μg of agonistic anti-CD137 or isotype control mAb was administered by an i.p. route. (B) Immune cell reconstitution was confirmed in recipient mice. The number of PNA$^+$CD95$^+$ GC B cells (C, E, and G) in the spleen at 14 dpi was determined. (F and G) Four-week-old TCRββ$^{-/-}$ mice were administered 7.1×10^6 WT CD4$^+$ T cells + WT CD8$^+$ T cells, WT CD4$^+$ T cells + CD137$^{-/-}$ CD8$^+$ T cells, CD137$^{-/-}$ CD4$^+$ T cells + WT CD8$^+$ T cells, or CD137$^{-/-}$ CD4$^+$ T cells + CD137$^{-/-}$ CD8$^+$ T cells by an i.v. route. Five days later, recipient mice were inoculated with 10^3 FFU of CHIKV. At 2 dpi, 400 μg of agonistic anti-CD137 or isotype control mAb was administered by an i.p. route. Symbols represent individual mice, and bars indicate median values. Data are pooled from 3 to 4 independent experiments (Mann-Whitney test: ***$p < 0.001$; ****$p < 0.0001$; n.s., not significant).

Most cells expressing *Tnfrsf9*, the gene encoding CD137, were NK and T cells (Figure S2B), which is consistent with results of our prior staining experiments by flow cytometry.[13] NK and T cells were reclustered to identify different cell subsets (e.g., NK cells, NKT cells, CD4$^+$ and CD8$^+$ T cells, and activated T cells) (Figures S2C and S2D). Among activated T cells, the frequency of cycling CD8$^+$ T cells, characterized by the expression of *Ccnb2*, *Ccna2*, *Cdca3,* and *Mki67* (Figure S3A), was increased in anti-CD137 mAb-treated mice compared to isotype control mAb-treated animals at 7 dpi. The cycling CD8$^+$ T cells and NK cells showed a proinflammatory and cytolytic signature with high transcript levels of *Gzma*, *Gzmb, Gzmk*, and *Ccl5* (Figures S3B and S3C). We also observed an expansion of myeloid cell subsets with proinflammatory signatures in anti-CD137 mAb-treated mice. For example, a subset of *S100a8/Mmp9*-expressing neutrophils (Figures S3D and S3E) expressed *Cxcl2*, *Il1b*, *Ccl6*, *Csf1*, *Tnf*, *Tnfsf14*, and *Il15* at higher levels at 7 dpi in anti-CD137 mAb-treated mice than the controls (Figures S3F and S3G). Clustered with the *Ccr2*-expressing monocytes were differentiating monocytes expressing *Spic*, a marker of red pulp macrophages[19] (Figures S3H and S3I). Differentiating monocytes persisted in anti-CD137 but not isotype control mAb-treated mice at 7 dpi and expressed higher transcript levels of the chemokines *Cxcl10*, *Cxcl9*, *Ccl2*, *Cxcl16*, and *Ccr5* (Figures S3J and S3K). Thus, scRNA-seq analysis revealed an expansion of several lymphoid and myeloid cell populations with proinflammatory signatures in anti-CD137 mAb-treated mice.

Anti-CD137 mAb Treatment Alters the Number of Tfh, Regulatory T, and Tfr Cells

scRNA-seq analysis revealed an activated CD4$^+$ T cell subset expressing genes (*Cxcr5* and *Il21*) characteristic of Tfh cells (Figure S4A).[20] Both scRNA-seq and flow cytometric data showed that at 7 dpi anti-CD137 mAb treatment resulted in a reduced frequency and number of CXCR5^{hi}PD-1^{hi} GC Tfh cells[21–23] (2.1-fold, $p < 0.0001$) (Figures S4B and S4C), which are essential for GC maintenance and affinity maturation.[12,24] We assessed whether the decreased number of GC Tfh cells in anti-CD137 mAb-treated mice was linked to the reduction of GC B cells. We rescued the number of GC Tfh cells by administering interleukin-2 (IL-2)-depleting and CTLA-4-blocking mAbs: IL-2

regulates Tfh cell differentiation by negatively modulating Bcl6 expression,[25] and CTLA-4 regulates Tfh cell differentiation by controlling the strength of CD28 signaling.[26] Combination treatment with IL-2-depleting and CTLA-4-blocking mAbs increased the number of GC Tfh cells in mice treated with anti-CD137 mAb to levels similar to those treated with isotype control mAb without treatment (Figure S4D). However, this treatment did not restore the number of GC B cells in anti-CD137 mAb-treated mice (Figure S4E). Thus, the decreased number of GC Tfh cells associated with anti-CD137 mAb treatment did not alone mediate the reduction in GC B cells.

scRNA-seq analysis also showed that anti-CD137 mAb treatment increased the proportion of $CD4^+$ and $CD8^+$ T cells expressing *Foxp3* (Figures S5A and S5C). Flow cytometric analysis at 2 dpi showed that most $CD4^+$ T cells expressing CD137 were $FoxP3^+$ Tregs (Figure S5D). Moreover, agonistic anti-CD137 mAb treatment increased the number and frequency of $CD4^+FoxP3^+$ Tregs (Figures S5E–S5G), $CD4^+CXCR5^{hi}PD\text{-}1^{hi}FoxP3^+$ Tfr cells (Figures S5H and S5I), and $CD8^+FoxP3^+$ T cells (Figures S5J and S5K). Because Tfr cells can modulate GC responses,[11] we used an adoptive transfer approach to assess whether the increased number of Tfr cells in anti-CD137 mAb-treated mice caused the reduction in GC B cells. T cells from $CD137^{-/-}$ mice and $FoxP3^+$ T cells sorted from FoxP3-GFP reporter mice were mixed and transferred into recipient $TCR\beta\delta^{-/-}$ mice (Figure S5L). Although Tregs and Tfr cells were reconstituted in recipient mice (Figure S5M), anti-CD137 mAb treatment failed to reduce the number of GC B cells at 14 dpi (Figure S5N). Thus, CD137 signaling exclusively on Tregs and Tfr cells among all T cell populations was not sufficient for anti-CD137 mAb-mediated reduction of GC B cells.

Anti-CD137 mAb Treatment Increases the Number of Antigen Nonspecific Plasmablasts and Minimally Alters BCR Usage

B cells were reclustered to identify different cell subsets (e.g., follicular B cells, marginal zone B cells, plasmablasts, and cycling B cells) (Figures S2C and S2D). Transcriptional analysis suggested that plasmablasts genes (*Xbp1*, *Irf4*, and *Prdm1*) were more abundant in anti-CD137 and isotype mAb-treated mice at 7 dpi than naive animals but more so in anti-CD137 mAb-treated animals (Figures 6A and 6B). Indeed, flow cytometry results of splenocytes showed that in anti-CD137 mAb-treated mice the total number of plasmablasts was increased at 7 dpi (2.1-fold, $p \leq 0.05$) but reduced at 14 dpi (2.9-fold, $p \leq 0.01$) (Figures 6C and 6D). In naive mice, anti-CD137 mAb treatment did not alter the number of plasmablasts in the spleen (Figure 6E).

During a primary GC reaction, naive B cells that bind to cognate antigens undergo somatic hypermutation and clonal selection, which biases the use of BCR genes in the pool of responding cells.[27] Because anti-CD137 mAb treatment disrupted the GC reaction, we evaluated whether anti-CD137 mAb treatment altered B cell clonality by analyzing the single-cell V(D)J sequences at 0 and 7 dpi. Overall, the BCR gene usage was similar between anti-CD137 mAb- and isotype control mAb-treated mice. Among the IgG clonotypes, *Igh2c* was used dominantly in both groups but not in naive animals (Figures S6A–S6D). There was bias in the use of *Ighv1-80* heavy chains joined with *Igkv5-39* or *Igkv5-43* light chains in both anti-CD137 and isotype control mAb-treated CHIKV-infected mice but not in naive animals (Figures S6A–S6C), suggesting that these genes were selected during acute CHIKV infection. There were minimal differences in V gene use of lambda light chains or J gene use among anti-CD137 and isotype control mAb-treated CHIKV-infected mice and naive animals (Figures S6A and S6D). Thus, BCR use seems minimally altered by anti-CD137 mAb treatment.

Even though there was an expansion of plasmablasts in anti-CD137 mAb-treated mice compared to isotype control mAb-treated animals, this did not occur at a clonal level (Figure S6E). Indeed, by enzyme-linked immunospot (ELISpot), we observed that the number of CHIKV-specific plasmablasts was similar between anti-CD137 mAb- and isotype control mAb-treated mice (Figure 6F). Thus, it appears that B cells with low or no affinity for CHIKV antigens prematurely differentiate into short-lived plasmablasts in anti-CD137 mAb-treated animals (Figure 6G).

Anti-CD137 mAb Treatment Negatively Impacts B Cell Responses in the Context of Viral Vaccine Immunization or Boosting

Memory Tfhs and FDCs within secondary lymphoid follicles promote the rapid differentiation of MBCs upon antigen re-encounter.[28–30] Because we observed that anti-CD137 mAb treatment disrupted secondary lymphoid follicles, we tested its effect on an anamnestic response to a vaccine antigen. Influenza virus HA is a well-defined antigen that elicits neutralizing antibodies.[31] Nine-week-old C57BL/6 female mice were immunized by an intramuscular route with influenza A virus H5 HA proteins (day 0) and then injected with anti-CD137 mAb 2 days later (Figure 7A). At 28 days postimmunization, the mice were boosted with H5 HA protein. The number of GC B cells, antigen-specific MBCs, and plasmablasts were reduced in anti-CD137 mAb-treated mice compared to isotype control mAb-treated animals 7 days after boosting (11.6-fold, $p < 0.001$; 30.5-fold, $p < 0.001$; 281-fold, $p < 0.001$, respectively) (Figures 7B–7D). In another group of mice, we administered anti-CD137 mAb 1 day before boosting to assess the effects on the anamnestic B cell response (Figure 7E). The numbers of GC B cells and antigen-specific MBCs but not antigen-specific plasmablasts were reduced in anti-CD137 mAb-treated mice compared to isotype control mAb-treated animals 7 days after boosting (12.9-fold, $p < 0.001$; 7.1-fold, $p < 0.001$; and not significant, respectively) (Figures 7F–7H). Thus, during an anamnestic memory response, anti-CD137 mAb treatment affects the secondary GC B cell and MBC response and has a minimal effect on plasmablast differentiation from pre-existing MBCs.

DISCUSSION

In this study, we have shown that administration of anti-CD137 mAb early (day 2) but not late (day 56) after CHIKV infection dampens the durable humoral immune response, as judged by marked reductions in antigen-specific MBCs, LLPCs, and serum antibody titers. Similarly, long-lasting antibody responses were impaired in response to NP-KLH, a T-cell-dependent antigen,

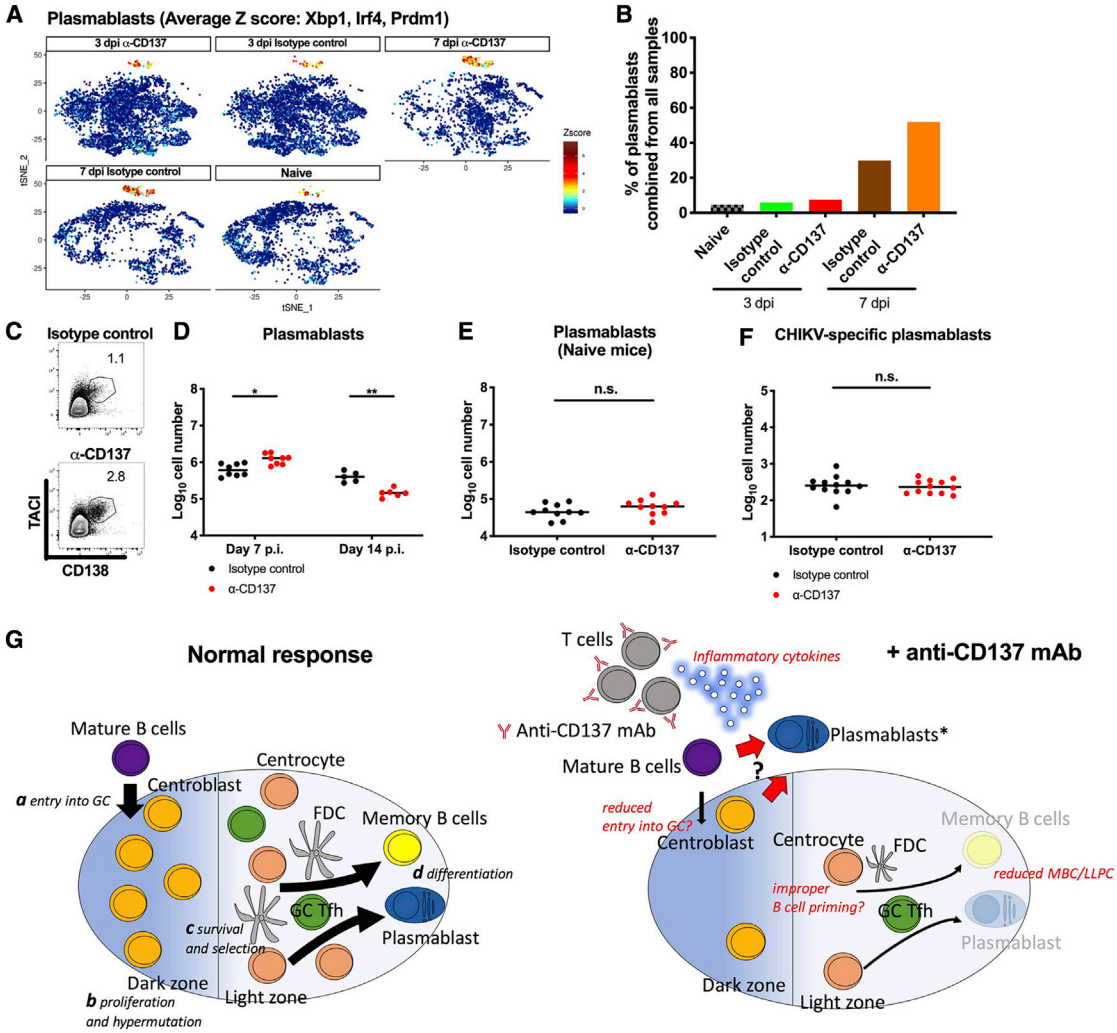

Figure 6. Anti-CD137 mAb Treatment Increases the Number of Plasmablasts

Four-week-old WT C57BL/6 male mice were inoculated with 10^3 FFU of CHIKV. At 2 dpi, 400 μg of agonistic anti-CD137 or isotype control mAb was administered by an i.p. route.

(A) Expression of *Xbp1*, *Irf4*, and *Prdm1* in plasmablasts is shown in t-distributed stochastic neighbor embedding (tSNE) plots.

(B) The fraction of plasmablasts combined from all samples is shown in bar graphs.

(C and D) $TACI^+CD138^+$ plasmablasts in the spleen at 7 dpi were analyzed by flow cytometry. (C) Representative dot plots and (D) total number of plasmablasts.

(E) Four-week-old naive WT C57BL/6 male mice were administered 400 μg of agonistic anti-CD137 or isotype control mAb by an i.p. route. The numbers of $TACI^+CD138^+$ plasmablasts in the spleen at 5 days after treatment were analyzed by flow cytometry.

(F) Four-week-old WT C57BL/6 male mice were inoculated with 10^3 FFU of CHIKV. At 2 dpi, 400 μg of agonistic anti-CD137 or isotype control mAb was administered by an i.p. route. The number of CHIKV-specific plasmablasts in the spleen at 7 dpi was analyzed by ELISpot. (D–F) Symbols represent individual mice, and bars indicate median values. Data are pooled from 3 independent experiments (Mann-Whitney test: $^*p < 0.05$; $^{**}p < 0.01$; n.s., not significant).

(G) Model of B cell differentiation after treatment with anti-CD137 mAb is shown. Left: in the context of normal T-cell-dependent responses, activated B cells enter GCs (*a*); proliferate and hypermutate in the dark zone (*b*); receive survival and selection signals from GC Tfh cells and FDCs (*c*); exit GCs as MBC, LLPCs, or plasmablasts (*d*). Right: the inflammatory environment induced by anti-CD137 mAb-activated T cells may induce B cells to differentiate prematurely into plasmablasts at the expense of GCs, which in combination with improper B cell priming due to altered B cell follicular architecture reduces the number of FDCs and GC Tfh cells that enable MBC and plasma cell differentiation. See also Figures S2, S3, S4, S5, and S6.

but not NP-Ficoll, a T-cell-independent antigen. The inhibition of the GC reaction in anti-CD137 mAb-treated mice was not associated with relatively increased cell death or decreased proliferation of GC B cells but was correlated with a disorganized architecture of the B cell follicle and disrupted VCAM-1 expression on FDCs. The anti-CD137 mAb-mediated effect on GC B cells required CD137 signaling in either $CD4^+$ or $CD8^+$ T cells. In addition to its effects on GC formation, anti-CD137 mAb treatment also increased the number of plasmablasts. Administration of anti-CD137 mAb prior to boosting with an influenza virus HA

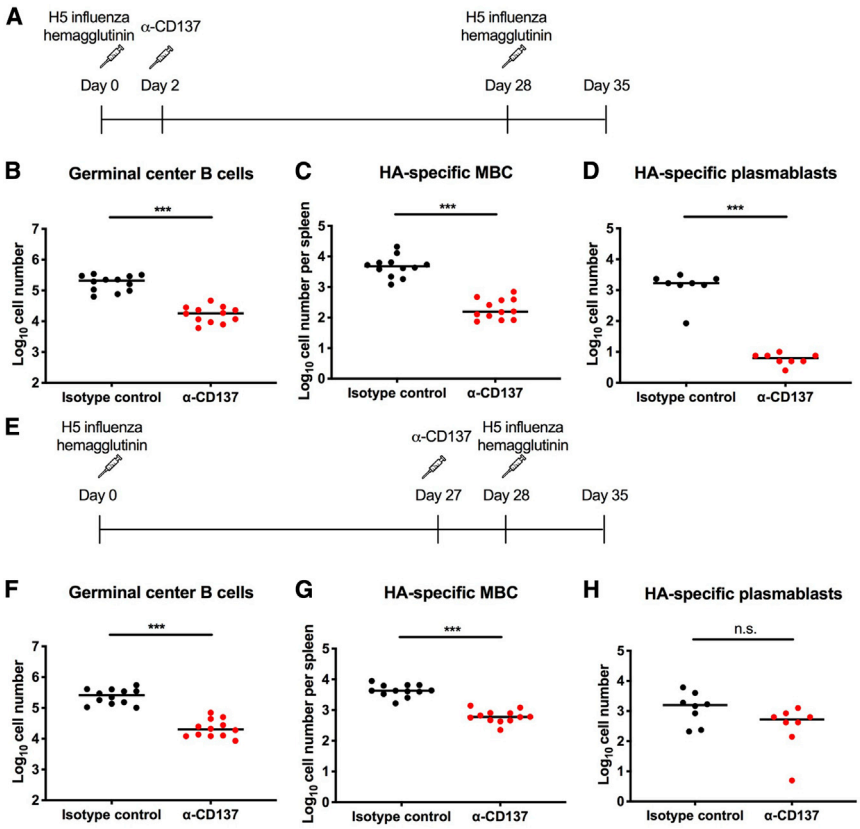

Figure 7. Effect of Anti-CD137 mAb Treatment on Antigen-Specific B Cell Populations when Administered before Viral Vaccine Boosting

Nine-week-old WT C57BL/6J female mice were injected by an intramuscular (i.m.) route with recombinant influenza A virus H5 HA protein. A total of 400 μg of agonistic anti-CD137 or isotype control mAb was administered by an i.p. route at either 2 days postimmunization (A) or 27 days postimmunization (E) before boosting with H5 HA at 28 days after initial immunization. Spleens were harvested 7 days after the booster immunization, and the numbers of GC B cells (B and F) and antigen-specific MBCs (C and G) were analyzed by flow cytometry. (D and H) The number of antigen-specific plasmablasts was analyzed by ELISpot. Symbols represent individual mice, and bars indicate median values. Data are pooled from 2 independent experiments (Mann-Whitney test: ***$p < 0.001$; n.s., not significant).

antigen reduced the secondary GC reaction but did not affect the differentiation of antigen-specific plasmablasts.

FDCs promote the expansion and maintenance of affinity-selected GC B cells by presenting antigens and interacting through their integrin proteins.[17,32,33] Our observations describing a disrupted B cell follicular architecture are consistent with an earlier report, which showed that anti-CD137 mAb treatment diminished GC formation and FDC networks, although that study was limited to immunohistochemistry analysis at 14 days after immunization with sheep erythrocytes and KLH.[34] Our imaging experiments show a diminished expression of VCAM-1 by FDCs, which is consistent with their lack of proper interaction and support for GC B cells. Because the proportion of GC B cells undergoing apoptosis or proliferation was similar between anti-CD137 and isotype control mAb-treated mice, we hypothesize that the inflammatory environment induced by anti-CD137 mAb-activated T cells results in improper GC B cell priming due to altered architecture, which in turn results in GC collapse and dispersal of activated B cells.

GCs are dynamic structures formed by antigen-specific B cells activated by cognate T cells. Somatic hypermutation and affinity-based selection occur in clonally expanding B cells, some of which egress from GC as plasma cells or MBCs. An alternative explanation for how anti-CD137 mAb alters the GC reaction is that some B cells with low or no affinity for viral antigens may differentiate prematurely into plasmablasts and exit. Indeed, we observed comparable numbers of CHIKV-specific plasmablasts in anti-CD137 and isotype control mAb-treated mice, even though the total number of plasmablasts was increased in anti-CD137 mAb-treated animals. Although anti-CD137 mAb treatment resulted in the short-term expansion of the plasmablast response, GC collapse led to a dampening of long-term antigen-specific antibody responses. We propose a model where the inflammatory environment induced by anti-CD137 mAb-activated T cells skews the differentiation of GC B cells. This results in the expansion of short-lived plasmablasts at the expense of GC reaction and also may lead to reductions in FDCs and GC Tfh cells (Figure 6G).

Anti-CD137 mAb when given at 2 days after the first immunization of influenza HA protein globally impaired anamnestic B cell responses at 7 days after the secondary booster immunization. However, when anti-CD137 mAb was given the day before boosting, the number of antigen-specific plasmablasts was not reduced, suggesting that this response does not require a secondary GC reaction. This is consistent with reports showing that re-entry of MBCs into germinal centers is rare under typical boost regimens.[35] After primary immunization, CXCR5-expressing memory Tfh cells accumulate at the B cell-T cell border and mediate efficient recall responses.[28,29] Upon encountering specific antigens during secondary infection or immunization, MBCs present the antigen to cognate $CD4^+$ T cells and proliferate and differentiate rapidly into plasmablasts.[28,36] Thus, when given before boosting, anti-CD137 mAb likely does not affect the interaction between MBCs and cognate memory Tfh cells. In contrast, anti-CD137 mAb likely hinders the secondary GC reaction of pre-existing MBCs. During the recall response, exogenous antigens bound by antibodies may be transported to FDCs, which then present immune complexes to MBCs for further rounds of affinity maturation and LLPC differentiation.[30] Because mice treated with anti-CD137 mAb show perturbed

GC architecture, secondary MBC differentiation likely becomes compromised.

Although agonistic anti-CD137 mAbs are being considered as therapies for cancer and autoimmune diseases,[1,37,38] their mechanism(s) of action remain unclear, and possible collateral effects on immune responses are understudied. Ligation of CD137 in DCs was reported to enhance the expression of retinal dehydrogenase, which induces the differentiation of FoxP3$^+$ Tregs.[7] In a mouse model of collagen-type-II-induced arthritis, anti-CD137 mAb treatment induced an expansion of CD11c$^+$CD8$^+$ T cells that produced interferon γ (IFNγ), which induced tolerogenic DCs.[8] We show that agonistic anti-CD137 mAb treatment inhibits humoral and cellular B cell responses, which could be another explanation for its utility in autoimmunity. Our data establish that T-cell-intrinsic signaling is required for CD137-dependent reduction in GC formation. This conclusion is consistent with a prior study showing that anti-CD137 mAb treatment diminished FDC networks in WT but not T-cell-deficient mice.[34] Although anti-CD137 mAbs are being tested in cancer clinical trials, no study has evaluated their effects on immune responses to viruses or vaccines. Our study establishes how anti-CD137 mAbs compromise the induction of memory responses in the B cell compartment but not the differentiation of pre-existing MBCs. In this respect, vaccination before anti-CD137 mAb therapy in humans may be beneficial. Although a corroborating analysis of human subjects is warranted, anti-CD137 mAb treatment in the context of immunotherapy could diminish or prevent antibody and memory responses to newly administered vaccines or infection with pathogens.

Limitations of Study

Although our study establishes potential collateral effects of anti-CD137 agonistic mAb therapy on GC formation and MBC induction, there are several qualifications: (1) the study was performed exclusively in mice and requires re-evaluation in humans, (2) there remains a gap in our understanding of how T cells activated by anti-CD137 antibody alter the architecture of the B cell follicle and skew differentiation of GC B cells, (3) a more granular kinetic analysis of the earliest consequences of anti-CD137 therapy on the FDC network could provide additional insight into the mechanism, and (4) the effects on B cells of anti-CD137 therapy were not explored in models of cancer or autoimmunity.

STAR★METHODS

Detailed methods are provided in the online version of this paper and include the following:

- KEY RESOURCES TABLE
- RESOURCE AVAILABILITY
  - Lead Contact
  - Materials Availability
  - Data and Code Availability
- EXPERIMENTAL MODEL AND SUBJECT DETAILS
  - Viruses and cells
  - Animal studies
- METHOD DETAILS
  - Antibodies and cell depletions
  - Immune cell analysis
  - Single cell RNA sequencing
  - Single cell RNA sequencing analysis
  - B cell clonal analysis
  - Immunofluorescence imaging
  - Adoptive transfer experiments
  - ELISA
  - MBC limiting dilution assay
  - ELISpot assay
  - Bone marrow transplantation
- QUANTIFICATION AND STATISTICAL ANALYSIS

SUPPLEMENTAL INFORMATION

Supplemental Information can be found online at https://doi.org/10.1016/j.xcrm.2020.100035.

ACKNOWLEDGMENTS

This work was supported by NIH grants R01 AI141436 (M.S.D.), NIAID Collaborative Influenza Vaccine Innovation Centers (CIVIC, 75N93019C00051), and the NIAID Centers of Excellence for Influenza Research and Surveillance (CEIRS, HHSN272201400008C). We thank Shirin Strohmeier for help in generating the recombinant H5 HA protein.

AUTHOR CONTRIBUTIONS

J.P.H. and M.S.D. conceived the study. J.P.H., G.R., A.S., and J.S.T. conducted the experiments. P.S.A., F.Z., and M.A. performed computational analysis of single-cell and B-cell RNA-seq data. A.C.M.B., F.K., and A.H.E. provided resources, reagents, and expertise with influenza immunization studies. H.D.H. supervised and analyzed the confocal microscopy studies. J.P.H. and M.S.D. wrote the first draft of the manuscript with all authors subsequently providing editorial input.

DECLARATION OF INTERESTS

M.S.D. is a consultant for Inbios and Emergent BioSolutions and on the Scientific Advisory Board of Moderna.

Received: December 12, 2019
Revised: March 10, 2020
Accepted: May 27, 2020
Published: June 23, 2020

REFERENCES

1. Yonezawa, A., Dutt, S., Chester, C., Kim, J., and Kohrt, H.E. (2015). Boosting Cancer Immunotherapy with Anti-CD137 Antibody Therapy. Clin. Cancer Res. *21*, 3113–3120.
2. Vinay, D.S., and Kwon, B.S. (2012). Immunotherapy of cancer with 4-1BB. Mol. Cancer Ther. *11*, 1062–1070.
3. Kocak, E., Lute, K., Chang, X., May, K.F., Jr., Exten, K.R., Zhang, H., Abdessalam, S.F., Lehman, A.M., Jarjoura, D., Zheng, P., and Liu, Y. (2006). Combination therapy with anti-CTL antigen-4 and anti-4-1BB antibodies enhances cancer immunity and reduces autoimmunity. Cancer Res. *66*, 7276–7284.
4. Westwood, J.A., Matthews, G.M., Shortt, J., Faulkner, D., Pegram, H.J., Duong, C.P., Chesi, M., Bergsagel, P.L., Sharp, L.L., Huhn, R.D., et al. (2014). Combination anti-CD137 and anti-CD40 antibody therapy in murine myc-driven hematological cancers. Leuk. Res. *38*, 948–954.
5. Takeda, K., Kojima, Y., Uno, T., Hayakawa, Y., Teng, M.W., Yoshizawa, H., Yagita, H., Gejyo, F., Okumura, K., and Smyth, M.J. (2010). Combination

therapy of established tumors by antibodies targeting immune activating and suppressing molecules. J. Immunol. *184*, 5493–5501.

6. Wei, H., Zhao, L., Li, W., Fan, K., Qian, W., Hou, S., Wang, H., Dai, M., Hellstrom, I., Hellstrom, K.E., and Guo, Y. (2013). Combinatorial PD-1 blockade and CD137 activation has therapeutic efficacy in murine cancer models and synergizes with cisplatin. PLoS One *8*, e84927.
7. Lee, S.W., Park, Y., Eun, S.Y., Madireddi, S., Cheroutre, H., and Croft, M. (2012). Cutting edge: 4-1BB controls regulatory activity in dendritic cells through promoting optimal expression of retinal dehydrogenase. J. Immunol. *189*, 2697–2701.
8. Seo, S.K., Choi, J.H., Kim, Y.H., Kang, W.J., Park, H.Y., Suh, J.H., Choi, B.K., Vinay, D.S., and Kwon, B.S. (2004). 4-1BB-mediated immunotherapy of rheumatoid arthritis. Nat. Med. *10*, 1088–1094.
9. Ascierto, P.A., Simeone, E., Sznol, M., Fu, Y.X., and Melero, I. (2010). Clinical experiences with anti-CD137 and anti-PD1 therapeutic antibodies. Semin. Oncol. *37*, 508–516.
10. Mesin, L., Ersching, J., and Victora, G.D. (2016). Germinal Center B Cell Dynamics. Immunity *45*, 471–482.
11. Linterman, M.A., Pierson, W., Lee, S.K., Kallies, A., Kawamoto, S., Rayner, T.F., Srivastava, M., Divekar, D.P., Beaton, L., Hogan, J.J., et al. (2011). Foxp3+ follicular regulatory T cells control the germinal center response. Nat. Med. *17*, 975–982.
12. Victora, G.D., and Nussenzweig, M.C. (2012). Germinal centers. Annu. Rev. Immunol. *30*, 429–457.
13. Hong, J.P., McCarthy, M.K., Davenport, B.J., Morrison, T.E., and Diamond, M.S. (2019). Clearance of Chikungunya virus infection in lymphoid tissues is promoted by treatment with an agonistic anti-CD137 antibody. J. Virol. *93*, e01231-19.
14. Bachmann, M.F., Odermatt, B., Hengartner, H., and Zinkernagel, R.M. (1996). Induction of long-lived germinal centers associated with persisting antigen after viral infection. J. Exp. Med. *183*, 2259–2269.
15. Mond, J.J., Lees, A., and Snapper, C.M. (1995). T cell-independent antigens type 2. Annu. Rev. Immunol. *13*, 655–692.
16. Akahata, W., Yang, Z.Y., Andersen, H., Sun, S., Holdaway, H.A., Kong, W.P., Lewis, M.G., Higgs, S., Rossmann, M.G., Rao, S., and Nabel, G.J. (2010). A virus-like particle vaccine for epidemic Chikungunya virus protects nonhuman primates against infection. Nat. Med. *16*, 334–338.
17. Wang, X., Rodda, L.B., Bannard, O., and Cyster, J.G. (2014). Integrin-mediated interactions between B cells and follicular dendritic cells influence germinal center B cell fitness. J. Immunol. *192*, 4601–4609.
18. Yao, Z., Jones, J., Kohrt, H., and Strober, S. (2011). Selective resistance of CD44hi T cells to p53-dependent cell death results in persistence of immunologic memory after total body irradiation. J. Immunol. *187*, 4100–4108.
19. Haldar, M., Kohyama, M., So, A.Y., Kc, W., Wu, X., Briseño, C.G., Satpathy, A.T., Kretzer, N.M., Arase, H., Rajasekaran, N.S., et al. (2014). Heme-mediated SPI-C induction promotes monocyte differentiation into iron-recycling macrophages. Cell *156*, 1223–1234.
20. Kuchen, S., Robbins, R., Sims, G.P., Sheng, C., Phillips, T.M., Lipsky, P.E., and Ettinger, R. (2007). Essential role of IL-21 in B cell activation, expansion, and plasma cell generation during CD4+ T cell-B cell collaboration. J. Immunol. *179*, 5886–5896.
21. Meli, A.P., Fontés, G., Avery, D.T., Leddon, S.A., Tam, M., Elliot, M., Ballesteros-Tato, A., Miller, J., Stevenson, M.M., Fowell, D.J., et al. (2016). The Integrin LFA-1 Controls T Follicular Helper Cell Generation and Maintenance. Immunity *45*, 831–846.
22. Shulman, Z., Gitlin, A.D., Targ, S., Jankovic, M., Pasqual, G., Nussenzweig, M.C., and Victora, G.D. (2013). T follicular helper cell dynamics in germinal centers. Science *341*, 673–677.
23. Trüb, M., Barr, T.A., Morrison, V.L., Brown, S., Caserta, S., Rixon, J., Ivens, A., and Gray, D. (2017). Heterogeneity of Phenotype and Function Reflects the Multistage Development of T Follicular Helper Cells. Front. Immunol. *8*, 489.
24. Baumjohann, D., Preite, S., Reboldi, A., Ronchi, F., Ansel, K.M., Lanzavecchia, A., and Sallusto, F. (2013). Persistent antigen and germinal center B cells sustain T follicular helper cell responses and phenotype. Immunity *38*, 596–605.
25. Ballesteros-Tato, A., León, B., Graf, B.A., Moquin, A., Adams, P.S., Lund, F.E., and Randall, T.D. (2012). Interleukin-2 inhibits germinal center formation by limiting T follicular helper cell differentiation. Immunity *36*, 847–856.
26. Wang, C.J., Heuts, F., Ovcinnikovs, V., Wardzinski, L., Bowers, C., Schmidt, E.M., Kogimtzis, A., Kenefeck, R., Sansom, D.M., and Walker, L.S. (2015). CTLA-4 controls follicular helper T-cell differentiation by regulating the strength of CD28 engagement. Proc. Natl. Acad. Sci. USA *112*, 524–529.
27. Kuraoka, M., Schmidt, A.G., Nojima, T., Feng, F., Watanabe, A., Kitamura, D., Harrison, S.C., Kepler, T.B., and Kelsoe, G. (2016). Complex Antigens Drive Permissive Clonal Selection in Germinal Centers. Immunity *44*, 542–552.
28. Aiba, Y., Kometani, K., Hamadate, M., Moriyama, S., Sakaue-Sawano, A., Tomura, M., Luche, H., Fehling, H.J., Casellas, R., Kanagawa, O., et al. (2010). Preferential localization of IgG memory B cells adjacent to contracted germinal centers. Proc. Natl. Acad. Sci. USA *107*, 12192–12197.
29. MacLeod, M.K., David, A., McKee, A.S., Crawford, F., Kappler, J.W., and Marrack, P. (2011). Memory CD4 T cells that express CXCR5 provide accelerated help to B cells. J. Immunol. *186*, 2889–2896.
30. Hanna, M.G., Jr., and Szakal, A.K. (1968). Localization of 125I-labeled antigen in germinal centers of mouse spleen: histologic and ultrastructural autoradiographic studies of the secondary immune reaction. J. Immunol. *101*, 949–962.
31. Impagliazzo, A., Milder, F., Kuipers, H., Wagner, M.V., Zhu, X., Hoffman, R.M., van Meersbergen, R., Huizingh, J., Wanningen, P., Verspuij, J., et al. (2015). A stable trimeric influenza hemagglutinin stem as a broadly protective immunogen. Science *349*, 1301–1306.
32. Endres, R., Alimzhanov, M.B., Plitz, T., Fütterer, A., Kosco-Vilbois, M.H., Nedospasov, S.A., Rajewsky, K., and Pfeffer, K. (1999). Mature follicular dendritic cell networks depend on expression of lymphotoxin beta receptor by radioresistant stromal cells and of lymphotoxin beta and tumor necrosis factor by B cells. J. Exp. Med. *189*, 159–168.
33. Luo, W., Weisel, F., and Shlomchik, M.J. (2018). B Cell Receptor and CD40 Signaling Are Rewired for Synergistic Induction of the c-Myc Transcription Factor in Germinal Center B Cells. Immunity *48*, 313–326.e315.
34. Sun, Y., Blink, S.E., Chen, J.H., and Fu, Y.X. (2005). Regulation of follicular dendritic cell networks by activated T cells: the role of CD137 signaling. J. Immunol. *175*, 884–890.
35. Mesin, L., Schiepers, A., Ersching, J., Barbulescu, A., Cavazzoni, C.B., Angelini, A., Okada, T., Kurosaki, T., and Victora, G.D. (2020). Restricted Clonality and Limited Germinal Center Reentry Characterize Memory B Cell Reactivation by Boosting. Cell *180*, 92–106.e111.
36. Kurosaki, T., Kometani, K., and Ise, W. (2015). Memory B cells. Nat. Rev. Immunol. *15*, 149–159.
37. Foell, J., Strahotin, S., O'Neil, S.P., McCausland, M.M., Suwyn, C., Haber, M., Chander, P.N., Bapat, A.S., Yan, X.J., Chiorazzi, N., et al. (2003). CD137 costimulatory T cell receptor engagement reverses acute disease in lupus-prone NZB x NZW F1 mice. J. Clin. Invest. *111*, 1505–1518.
38. Mittler, R.S., Foell, J., McCausland, M., Strahotin, S., Niu, L., Bapat, A., and Hewes, L.B. (2004). Anti-CD137 antibodies in the treatment of autoimmune disease and cancer. Immunol. Res. *29*, 197–208.
39. Tsetsarkin, K., Higgs, S., McGee, C.E., De Lamballerie, X., Charrel, R.N., and Vanlandingham, D.L. (2006). Infectious clones of Chikungunya virus (La Réunion isolate) for vector competence studies. Vector Borne Zoonotic Dis. *6*, 325–337.
40. Pal, P., Dowd, K.A., Brien, J.D., Edeling, M.A., Gorlatov, S., Johnson, S., Lee, I., Akahata, W., Nabel, G.J., Richter, M.K., et al. (2013). Development

of a highly protective combination monoclonal antibody therapy against Chikungunya virus. PLoS Pathog. *9*, e1003312.

41. Kwon, B.S., Hurtado, J.C., Lee, Z.H., Kwack, K.B., Seo, S.K., Choi, B.K., Koller, B.H., Wolisi, G., Broxmeyer, H.E., and Vinay, D.S. (2002). Immune responses in 4-1BB (CD137)-deficient mice. J. Immunol. *168*, 5483–5490.
42. Ellebedy, A.H., Krammer, F., Li, G.M., Miller, M.S., Chiu, C., Wrammert, J., Chang, C.Y., Davis, C.W., McCausland, M., Elbein, R., et al. (2014). Induction of broadly cross-reactive antibody responses to the influenza HA stem region following H5N1 vaccination in humans. Proc. Natl. Acad. Sci. USA *111*, 13133–13138.
43. Wilcox, R.A., Flies, D.B., Zhu, G., Johnson, A.J., Tamada, K., Chapoval, A.I., Strome, S.E., Pease, L.R., and Chen, L. (2002). Provision of antigen and CD137 signaling breaks immunological ignorance, promoting regression of poorly immunogenic tumors. J. Clin. Invest. *109*, 651–659.
44. Butler, A., Hoffman, P., Smibert, P., Papalexi, E., and Satija, R. (2018). Integrating single-cell transcriptomic data across different conditions, technologies, and species. Nat. Biotechnol. *36*, 411–420.
45. Dobin, A., Davis, C.A., Schlesinger, F., Drenkow, J., Zaleski, C., Jha, S., Batut, P., Chaisson, M., and Gingeras, T.R. (2013). STAR: ultrafast universal RNA-seq aligner. Bioinformatics *29*, 15–21.
46. Anders, S., Pyl, P.T., and Huber, W. (2015). HTSeq—a Python framework to work with high-throughput sequencing data. Bioinformatics *31*, 166–169.
47. Traag, V.A., Waltman, L., and van Eck, N.J. (2019). From Louvain to Leiden: guaranteeing well-connected communities. Sci. Rep. *9*, 5233.
48. Purtha, W.E., Tedder, T.F., Johnson, S., Bhattacharya, D., and Diamond, M.S. (2011). Memory B cells, but not long-lived plasma cells, possess antigen specificities for viral escape mutants. J. Exp. Med. *208*, 2599–2606.

STAR★METHODS

KEY RESOURCES TABLE

REAGENT or RESOURCE	SOURCE	IDENTIFIER
Antibodies		
Anti-CD137 mAb 2A	Wilcox et al.[43]	N/A
Anti-IL-2 mAb S4B6-1	Bio X Cell	Cat#BE0043-1; RRID: AB_1107705
Anti-CTLA-4 mAb 9D9	Bio X Cell	Cat#BE0164; RRID: AB_10949609
Rat IgG2a 2A3	Bio X Cell	Cat#BE0089; RRID: AB_1107769
Mouse IgG2b MPC-11	Bio X Cell	Cat#BE0086; RRID: AB_1107791
Purified rat anti-mouse CD16/32 mAb	BioLegend	Cat#101302; RRID: AB_312801
BV605 conjugated rat anti-mouse CD45 mAb	BioLegend	Cat#103140; RRID: AB_2562342
PE/Cy7 conjugated Armenian hamster anti-mouse CD3ε mAb	BioLegend	Cat#100320; RRID: AB_312685
APC/Cy7 conjugated rat anti-mouse CD19 mAb	BioLegend	Cat#115530; RRID: AB_830707
FITC conjugated rat anti-mouse CD21/CD35 mAb	BD Biosciences	Cat#553818; RRID: AB_395070
PE conjugated Armenian hamster anti-mouse CD95 mAb	BD Biosciences	Cat#554258; RRID: AB_395330
Alexa647 conjugated rat anti-mouse FoxP3 mAb	BioLegend	Cat#126408; RRID: AB_1089115
Biotinylated rat anti-mouse CXCR5 mAb	BioLegend	Cat#145510; RRID: AB_2562126
BV421 conjugated rat anti-mouse CD4 mAb	BioLegend	Cat#100438; RRID: 11203718
PerCP/Cy5.5 conjugated rat anti-mouse CD8α mAb	BioLegend	Cat#100734; RRID: 2075238
Alexa647 conjugated rat anti-mouse CD86 mAb	BioLegend	Cat#105019; RRID: AB493465
PE conjugated rat anti-mouse CXCR4 mAb	BioLegend	Cat#146505; RRID: AB_2562782
FITC conjugated rat anti-mouse PD-1 mAb	BioLegend	Cat#135214; RRID: AB_10680238
BV510 conjugated mouse anti-mouse CD45.1 mAb	BioLegend	Cat#110741; RRID: AB_2563378
Alexa700 conjugated mouse anti-mouse CD45.2 mAb	Thermo	Cat#56-0454-82; RRID: AB_657752
Alexa647 conjugated rat anti-mouse CD138 mAb	BioLegend	Cat#142526; RRID: AB_2566239
BV421 conjugated rat anti-mouse TACI mAb	BD Biosciences	Cat#742840; RRID: AB_2741091
Biotinylated goat polyclonal anti-mouse IgG	Sigma	Cat#B7022; RRID: AB_258598
BV421 conjugated rat anti-mouse IgM mAb	BioLegend	Cat#406517; RRID: AB_10899576
Alexa647 conjugated rat anti-mouse CD38 mAb	BioLegend	Cat#102716; RRID: AB_2073334
BV510 conjugated rat anti-mouse IgD mAb	BioLegend	Cat#405723; RRID: AB_2562742
PerCP/Cy5.5 conjugated rat anti-mouse, human GL7 mAb	BioLegend	Cat#144609; RRID: AB_2562978
Biotinylated Syrian hamster anti-mouse CD137 mAb	BioLegend	Cat#106104; RRID: AB_313241
Purified rat anti-reticular fibroblasts and reticular fibers mAb	Abcam	Cat#ab51824; RRID: 881651
Purified rabbit anti-mouse CD4 mAb	Abcam	Cat#ab183685; RRID: AB_2686917
Alexa555 conjugated goat polyclonal anti-rabbit IgG (H+L)	Thermo	Cat#A-21428; RRID: AB_141784
Alexa700 conjugated rat anti-B220 mAb	BioLegend	Cat#103232; RRID: AB_493717
Alexa647 conjugated rat anti-mouse, human GL7	BioLegend	Cat#144606; RRID: AB_2562185
Alexa647 conjugated donkey polyclonal anti-goat IgG (H+L)	Thermo	Cat#A-21447; RRID: AB_141844
Biotinylated rat anti-mouse IgD mAb	SouthernBiotech	Cat#1120-08; RRID: AB_2631189
eFluor450 rat anti-mouse CD21/CD35 mAb	Thermo	Cat#48-0212-82; RRID: AB_2016703
Biotinylated goat polyclonal anti-mouse IgG (H+L)	Jackson ImmunoResearch	Cat#115-065-062; RRID: AB_2338562
Purified rat anti-mouse VCAM-1 mAb	Thermo	Cat#14-1061-85; RRID: AB_467420
Bacterial and Virus Strains		
Chikungunya virus (strain LR-2006)	Tsetsarkin et al.[39]	KY575571
Chemicals, Peptides, and Recombinant Proteins		
Biotinylated peanut agglutinin	Vector	Cat#B-1075; RRID: AB_2313597
Alexa647 conjugated streptavidin	Thermo	Cat#S-21374; RRID: AB_2336066

(*Continued on next page*)

Continued

REAGENT or RESOURCE	SOURCE	IDENTIFIER
PE conjugated 4-Hydroxy-3-nitrophenylacetyl hapten	Biosearch Technologies	Cat# N-5070-1
Biotinylated H5	Immune Technology	Cat# IT-003-0052ΔTMp
Alexa555 conjugated streptavidin	Thermo	Cat#S32355; RRID: AB_2571525
4-Hydroxy-3-nitrophenylacetyl hapten conjugated Ficoll	Biosearch Technologies	Cat#F-1420-10
4-Hydroxy-3-nitrophenylacetyl hapten conjugated Keyhole Limpet Hemocyanin	Biosearch Technologies	Cat#N-5060-5
Alum adjuvant	Thermo	Cat#77161
AddaVax adjuvant	InvivoGen	Cat#vac-adx-10
Recombinant H5 hemagglutinin	Ellebedy et al.[42]	N/A
Recombinant chikungunya virus E2 protein	Pal et al.[40]	N/A
4-Hydroxy-3-nitrophenylacetyl hapten conjugated chicken gamma globulin	Biosearch Technologies	Cat#N-5055E-5
Streptavidin conjugated horseradish peroxidase	Vector	Cat#SA-5004; RRID: AB_2336509
Chikungunya virus-like particles (strain 37997)	Akahata et al.[16]	N/A
Critical Commercial Assays		
eFluor506 fixable viability dye	Thermo	Cat#65-0866-14
annexin V detection kit eFluor450	Thermo	Cat#88-8006-72
FITC Brdu flow kit	BD Biosciences	Cat#559619; RRID: AB_2617060
$CD4^+$ T cell isolation kit	Miltenyi Biotec	Cat#130-104-454
$CD8\alpha^+$ T cell isolation kit	Miltenyi Biotec	Cat#130-104-075
Pan T cell isolation kit	Miltenyi Biotec	Cat#130-090-130
Chromium Single Cell 5′ Library & Gel Bead Kit	10x Genomics	Cat#1000006
Chromium Single Cell 5′ Library Construction Kit	10x Genomics	Cat#1000020
Chromium Single Cell A Chip Kit	10x Genomics	Cat#120236
Chromium Single Cell V(D)J Enrichment Kit, Mouse B Cell	10x Genomics	Cat#1000072
Chromium i7 Multiplex Kit	10x Genomics	Cat#120262
Deposited Data		
Single cell RNA sequencing data – gene expression	This study	GEO: GSE141111
Single cell RNA sequencing data – BCR V(D)J	This study	GEO: GSE141117
B cell clonal analysis code	This study	https://github.com/iosonofabio/BCR_Zanini_Diamond
Experimental Models: Organisms/Strains		
Mouse: C57BL/6J	Jackson Laboratory	Cat#000664; RRID: IMSR_JAX:000664
Mouse: B6.129P2-$Tcrb^{tm1Mom}$ $Tcrd^{tm1Mom}$/J	Jackson Laboratory	Cat#002121; RRID: IMSR_JAX:002121
Mouse: C.Cg-$Foxp3^{tm2Tch}$/J	Jackson Laboratory	Cat#006769; RRID: IMSR_JAX:006769
Mouse: B6.SJL-$Ptprc^a$ $Pepc^b$/BoyJ	Jackson Laboratory	Cat#002014; RRID: IMSR_JAX:002014
Mouse: $CD137^{-/-}$	Kwon et al.[41]	N/A
Software and Algorithms		
FACSDiva	BD Biosciences	N/A
FlowJo	FlowJo, LLC	N/A
GraphPad Prism	GraphPad	N/A

RESOURCE AVAILABILITY

Lead Contact

Further information and requests for resources and reagents should be directed to and will be fulfilled by the Lead Contact, Michael S. Diamond (diamond@wusm.wustl.edu).

Materials Availability

All requests for resources and reagents should be directed to and will be fulfilled by the Lead Contact author. This includes transgenic mice, antibodies, and proteins. Antibodies to CD137 and CD137$^{-/-}$ mice will be made available on request after completion of a Materials Transfer Agreement.

Data and Code Availability

The authors declare that all data supporting the findings of this study are available within the paper. All sequencing data have been deposited as GSE141111 and GSE141117.

EXPERIMENTAL MODEL AND SUBJECT DETAILS

Viruses and cells

The recombinant CHIKV La Reunion OPY1 strain was generated from a full-length infectious cDNA clone using T7-dependent DNA-dependent RNA polymerase *in vitro* transcription, and transfection of viral RNA into BHK-21 cells, as described previously.[39] The resultant virus was harvested from the supernatant, propagated once in C6/36 *Aedes albopictus* cells, and titrated using Vero cells and a focus-forming assay as described.[40]

Animal studies

All animal experiments were performed with the approval of Washington University Institutional Animal Care and Use Committee guidelines. All mouse infection studies were performed in an animal biosafety level 3 laboratory. C57BL/6J (000664), B6.129P2-Tcrb^{tm1Mom} Tcrd^{tm1Mom}/J (002121; abbreviated TCR$\beta\delta^{-/-}$), C.Cg-Foxp3^{tm2Tch}/J (006769; abbreviated FoxP3-GFP) and B6.SJL-Ptprc^{a} Pepc^{b}/BoyJ (002014) were purchased from Jackson Laboratories. CD137$^{-/-}$ mice[41] were obtained as a gift from Michael Croft (La Jolla Institute for Immunology). At 4 weeks of age, male mice were anesthetized with ketamine hydrochloride (80 mg/kg) and xylazine (15 mg/kg) and inoculated s.c. in the left rear footpad with 10^3 focus-forming units (FFU) of CHIKV in 10 μL of PBS. For immunization with NP-Ficoll (Biosearch Technologies) or NP-KLH (Biosearch Technologies), 4-week-old C57BL/6J male mice were injected via i.p. route with 5 μg of NP-Ficoll in 200 μL of PBS or 10 μg of NP-KLH in 100 μL of alum mixture (1:1 ratio of immunogen in PBS to alum (Thermo)). For immunization with influenza A virus H5 hemagglutinin, 9-week-old C57BL/6J female mice were injected via intramuscular (i.m.) route with 10 μg of recombinant H5 HA[42] in 50 μL of antigen:AddaVax (1:1) (InvivoGen). At the termination of experiments, mice were euthanized and perfused via intracardiac injection with PBS. For proliferation assays, CHIKV-infected mice were injected via intravascular route with 1 mg of Brdu in 100 μL of PBS two hours before harvest.

METHOD DETAILS

Antibodies and cell depletions

Anti-CD137 mAb (clone 2A, rat Ig2a) has been described previously.[43] Antibody was purified from hybridoma supernatants by protein G affinity chromatography by a commercial vendor (BioXCell). Anti-IL-2 (clone S4B6-1) and anti-CTLA-4 (clone 9D9) were purchased from BioXCell and used for IL-2 depletion and CTLA-4 blockade, respectively, with rat IgG2a (clone 2A3) and mouse IgG2b (clone MPC-11) serving as isotype controls. Mice were administered 400 μg of anti-CD137 or rat Ig2a isotype control mAb (clone 2A3, BioXCell) via i.p. route at 2 dpi. For IL-2 depletion studies, mice were administered 500 μg of anti-IL-2 mAb on 2, 4 and 6 dpi. For CTLA-4 blockade, mice were administered 500 μg of anti-CTLA-4 mAb on 2 dpi and 250 μg on 5 dpi.

Immune cell analysis

Spleens were minced and incubated for 30 min at 37°C in 2 mL digestion buffer (1 mg/ml collagenase (Sigma) and 100 μg/mL DNase I (Sigma) in Dulbecco's Modified Eagle's medium (DMEM) containing 2% FBS in a 24-well plate. Cell suspensions were passed through a 100 μm cell strainer. After rinsing with 10% FBS, 5 mM EDTA in DMEM, erythrocytes were lysed with 1 mL of ACK Lysing Buffer (GIBCO) per spleen for 2 min. Cells were washed with DMEM and centrifuged, followed by rinsing with washing buffer (2% FBS, 5 mM EDTA in PBS). After centrifugation, cells were resuspended in washing buffer at 5×10^8 cells/ml and incubated with 2.5 μg of anti-mouse CD16/32 antibody (101302, Biolegend) per 10^8 cells for 20 min on ice. Then, cells were stained with BV605-conjugated anti-CD45 (103140, Biolegend), PE-Cy7-conjugated anti-CD3 (100320, Biolegend), APC-Cy7-conjugated anti-CD19 (115530, Biolegend), FITC-conjugated anti-CD21/35 (553818, BD Biosciences), PE-conjugated anti-CD95 (554258, BD Biosciences), Alexa647-conjugated anti-FoxP3 (126408, Biolegend), biotinylated anti-CXCR5 (145510, BIolegend), BV421-conjugated anti-CD4 (100438, Biolegend), PerCP/Cy5.5-conjugated anti-CD8α (100734, Biolegend), Alexa647-conjugated anti-CD86 (105019, Biolegend), PE-conjugated anti-CXCR4 (146505, Biolegend), FITC-conjugated anti-PD-1 (135214, Biolegend), BV510-conjugated anti-CD45.1 (110741, Biolegend), Alexa700-conjugated anti-CD45.2 (56-0454-82, Thermo), Alexa647-conjugated anti-CD138 (142526, Biolegend), BV421-conjugated anti-TACI (742840, BD Biosciences), biotinylated anti-IgG (B7022, Sigma), BV421-conjugated anti-IgM (406517, Biolegend), Alexa647-conjugated anti-CD38 (102716, Biolegend), BV510-conjugated anti-IgD (405723, Biolegend), PerCP/Cy5.5-conjugated anti-GL7 (144609, Biolegend) antibody, biotinylated PNA (B-1075, Vector), Alexa647-conjugated streptavidin (S-21374, Thermo) and eFluor506 fixable viability dye (65-0866-14, Thermo). For detection of

apoptosis, an annexin V detection kit eFluor450 (88-8006-72, Thermo) was used according to the manufacturer's instructions. For proliferation detection, the Brdu flow kit (559619, BD) was used according to the manufacturer's instructions. To confirm CD137 expression, cells were stained with biotinylated anti-CD137 (106104, Biolegend). For detection of NP-specific and hemaglutinin-specific memory B cells, cells were stained sequentially with PE-conjugated NP (N-5070-1, Biosearch Technologies) or biotinylated H5 (IT-003-0052ΔTMp, Immune Technology). Subsequently, cells were fixed with BD FACS Lysing Solution, processed on a LSR Fortessa X-20 (BD Biosciences) flow cytometer, and analyzed using BD FACSDiva and FlowJo software.

Single cell RNA sequencing

Isolated single cell suspensions were subjected to droplet-based massively parallel single cell RNA sequencing using Chromium Single Cell 5′ Reagent Kit in a BSL-3 level laboratory as per manufacturer's instructions (10x Genomics). Briefly, cell suspensions were loaded at 1,000 cells/μL with the aim to capture 10,000 cells/well. The 10x Chromium Controller generated GEM droplets, where each cell was labeled with a specific barcode, and each transcript labeled with a unique molecular identifier (UMI) during reverse transcription. The barcoded cDNA was isolated via a Dynabeads MyOne SILANE bead cleanup mixture and amplified 13 cycles. Amplified cDNA was purified via SPRI bead cleanup and removed from the BSL-3 space for library generation. For gene expression libraries, 50 ng of amplified cDNA was used for library preparation, consisting of fragmentation, end repair, A-tailing, adaptor ligation and sample index PCR as per the manufacturer's instructions. Libraries were sequenced on a NovaSeq S4 (200 cycle) flow cell, targeting 45,000 read pairs/cell. For B Cell repertoire libraries, 2 μL of amplified cDNA underwent two rounds of Target Enrichment using nested primer pairs specific for mouse B cell Ig constant regions. 50 ng of the target enrichment PCR product was used for library preparation, consisting of fragmentation, end repair, A-tailing, adaptor ligation and sample index PCR as per the manufacturer's instructions. Enriched libraries were sequenced on a NovaSeq S4 (200 cycle) flow cell, targeting 5,000 read pairs/cell. All sequencing data have been submitted to the GEO database (GSE141111 and GSE141117).

Single cell RNA sequencing analysis

Sample demultiplexing, barcode processing, and single-cell 5′ counting was performed using the Cell Ranger Single-Cell Software Suite (10x Genomics). Cellranger count was used to align samples to the mm10 reference genome, quantify reads, and filter reads with a quality score below 30. The resultant files were input into Seurat for normalization across all samples and merging. The Seurat package in R was used for subsequent analysis.[44] Cells with mitochondrial content greater than 5 percent were removed for downstream analysis. Data were normalized using a scaling factor of 10,000, and number of Unique Molecular Identifiers was regressed with a negative binomial model. Principal component analysis was performed using the top 3,000 most variable genes and t-SNE analysis was performed with the top 10 PCAs. Clustering was performed using the FindClusters function which works on K-nearest neighbor graph model with the granularity ranging from 0.1-0.9 and selected 0.6 for the downstream clustering. For identifying the markers for each cluster, we performed differential expression of each cluster against all other clusters identifying negative and positive markers for that cluster. Data from different cell types (*e.g.*, NK cells/T cells and B cells) were re-clustered to further analyze transcripts in each cell type.

B cell clonal analysis

The sequencing reads were preprocessed using 10X Genomics' cellranger vdj package. The B cell receptor (BCR) sequences were assembled using the mouse IMGT database and variable V, J, and constant chain alleles were called for both heavy and light chain. BCRs with identical CDR3 nucleotide sequences were assigned to the same clonal family irrespective of their V, J, and constant region calls, which are the standard parameters. Among all sequenced cells, B cells were identified by transcriptome analysis. Briefly, reads were mapped against the *Mus musculus* genome (mm10-3.0.0) using cellranger count, which included STAR aligner[45] and HTSeq.[46] The gene expression table was restricted to the 500 genes with the highest Fano factor and log transformed. PCA with 30 components was then used to reduce dimensionality, pairwise correlation distances were then used to construct a k-nearest neighbor graph with k = 15 and a threshold for edge calling of $\geq$ 0.2. Unsupervised clustering on the graph was performed using Leiden,[47] constant Potts model optimization, and a resolution parameter of 0.001. Clonal analysis was performed for heavy and light chains separately. Clonal graph plots were restricted to families with $\geq$ 2 members. All plots were generated via custom Python 3.7 scripts. The code for the whole B cell clonal analysis is available at https://github.com/iosonofabio/BCR_Zanini_Diamond.

Immunofluorescence imaging

Spleens were fixed in periodate-lysine-paraformaldehyde buffer for 48 h, and moved to 30% sucrose in PBS for at least 24 h before embedding. Tissues were embedded in optimal-cutting-temperature medium (Electron Microscopy Sciences) in longitudinal orientation and frozen in dry-ice-cooled isopentane. 18-μm sections were cut on a Lecia cryostat (Leica Microsystems), blocked with 10% bovine and donkey serum, and then stained with combinations of the following antibodies: anti-reticular fibroblasts and reticular fibers (ab51824, Abcam), anti-CD21/35 (48-0212-82, Thermo), anti-CD4 (ab183685, Abcam), Alexa555-conjugated anti-rabbit IgG (A-21428, Thermo), Alexa700-conjugated anti-B220 (103232, Biolegend), Alexa647-conjugated anti-GL7 (144606, Biolegend), Alexa647-conjugated anti-goat IgG (A-21447, Thermo), biotinylated anti-IgD (1120-08, SouthernBiotech) antibody and Alexa555-conjugated streptavidin (S32355, Thermo). Images were acquired on a Leica SP8 confocal microscope equipped with acousto-optical tunable filters, HyD hybrid detectors, and a 700 nm wavelength laser (Leica Microsystems). Images were merged from tilescans

acquired with a 40X objective. Images were processed and analyzed using Imaris (Bitplane). FDC area was calculated using the "Surfaces" function of Imaris and measured only FDCs networks in follicles that contained FDCs. GC B cells were marked using the automated "Spots" function of Imaris. The percentage of GC B cells far away from FDCs were calculated using the Imaris XT module "Spots and Surfaces Distance." GC B cells were considered far away from FDCs if they were greater than 10 μm from the closest FDC surface. The distance between GC B cells was calculated using the Imaris XT module "Spots to Spots Closest Distance."

Adoptive transfer experiments

Minced spleens from naive WT or CD137$^{-/-}$ mice were passed through a 70 μm cell strainer to generate single cell splenocyte suspensions. After lysis of erythrocytes, CD4$^+$ and CD8$^+$ T cells were isolated using the CD4$^+$ or CD8α$^+$ T Cell Isolation Kits (130-104-454 and 130-104-075, respectively, Miltenyi Biotec) according to the manufacturer's instructions. 4.3 × 10^6 CD4$^+$ T cells and 2.8 × 10^6 CD8$^+$ T cells were mixed and adoptively transferred into TCRβδ$^{-/-}$ mice. After 5 days, the recipient mice were inoculated with 10^3 FFU of CHIKV. For adoptive transfer of FoxP3$^+$ T cells, spleens from naive CD137$^{-/-}$ mice and FoxP3-GFP reporter mice were processed as described above. T cells were isolated using the Pan T Cell Isolation Kit (130-090-130, Miltenyi Biotec). The isolated T cells were sorted using a BD FACS Aria II. 1.3 × 10^5 sorted FoxP3$^+$ T cells and 7.1 × 10^6 CD137$^{-/-}$ T cells were adoptively transferred into TCRβδ$^{-/-}$ mice.

ELISA

MaxiSorp 96-well flat-bottom ELISA plates (44-2404-21, Thermo) were coated with 2 μg/ml of CHIKV E2 protein[40] or 20 μg/ml of NP-conjugated chicken gamma globulin (NP-CGG, Biosearch Technologies) overnight at 4°C. Plates were washed with ELISA wash buffer (PBS, 0.05% Tween-20) and then incubated with blocking buffer (PBS, 5% FBS) for 4 h at 37°C. Sera from CHIKV-infected, NP-KLH- or NP-Ficoll-immunized mice were added in 3-fold dilutions starting with a 1/100 dilution. After incubating for 1 h at room temperature, plates were rinsed with ELISA wash buffer and then incubated with biotinylated anti-IgG (115-065-062, Jackson ImmunoResearch) for 1 h at room temperature. After washing, plates were incubated with streptavidin-conjugated HRP (SA-5004, Vector Laboratories) for 30 min at room temperature. After final rinses with ELISA wash buffer and PBS, substrate solution (34029, Thermo) was added. The reaction was quenched with 2N H_2SO_4, and the plates were read using a Synergy H1 Hybrid Reader (BioTek). The optical density (OD) value of naive serum was subtracted from OD values of CHIKV-infected or NP-Ficoll- or NP-KLH-immunized samples, and non-linear regression curves were calculated. The titer of anti-CHIKV or anti-NP was defined as the dilution of serum yielding a half-maximal OD value after background and naive value subtraction.

MBC limiting dilution assay

96-well flat-bottom feeder cell plates were seeded with BAFF- and CD40L-expressing feeder cells the day before B cell isolation and were incubated with 5 μg/ml of mitomycin C at 37°C and 5% humidified CO2 for 3 h, as described before.[48] Splenocyte suspensions from CHIKV-infected mice were centrifuged and resuspended in washing buffer (1% FBS, 2 mM EDTA in PBS). CD19$^+$ B cells were isolated using CD19 MicroBeads (130-052-201, Miltenyi Biotec) according to the manufacturer's protocol. The isolated B cells were cultured (RPMI, 10% FBS, 1X penicillin-streptomycin, 1 mM sodium pyruvate, 0.1 mM non-essential amino acids, 10 mM HEPES, 50 μM β-mercaptoethanol) in 5-fold dilutions starting at 1,000,000 cells per well in the feeder cell plates sealed with an adhesive film at 37°C and 5% humidified CO_2 for 6 days. To calculate the frequency of CHIKV-specific MBCs that produced IgG, MaxiSorp 96-well flat-bottom ELISA plates (44-2404-21, Thermo) were coated with 2 μg/ml of CHIKV E2 protein[40] overnight at 4°C. Plates were washed with ELISA wash buffer (PBS, 0.05% Tween-20) and blocked with blocking buffer (PBS, 5% FBS) for 4 h at 37°C. Supernatants from B cell culture were added to the ELISA plates (50 μl per well) and processed as described above for serum antibodies. Positive wells were defined as wells that scored 2-fold over the mean OD of negative control wells (wells containing feeder cells and naive B cells). The frequency of CHIKV-specific MBCs was calculated as one cell per the number of cells plated where 63.2% of wells were positive.

ELISpot assay

Mixed cellulose filter 96-well plates (Millipore) plates were pre-coated with 50 μg/ml of CHIKV E2 protein,[40] 20 μg/ml of NP-CGG (Biosearch Technologies) or 2 μg/ml of H5[42] overnight at 4°C. After rinsing with ELISA wash buffer and PBS, plates were blocked for 4 h at 37°C with culture medium (RPMI, 10% FBS, penicillin-streptomycin, 1 mM sodium pyruvate, 0.1 mM non-essential amino acids, 10 mM HEPES, and 50 μM β-mercaptoethanol). For LLPC assays, bone marrow from the tibia and femur was filtered through 40 μm cell strainer. For plasmablast assays, single cell splenocyte suspensions were generated as detailed above. Erythrocytes were lysed, and CD138$^+$ cells were isolated using CD138 MicroBeads (130-098-257, Miltenyi Biotec). The isolated cells were incubated (RPMI 1640, 10% FBS, penicillin-streptomycin, 1 mM sodium pyruvate, 0.1 mM non-essential amino acids, 10 mM HEPES, 50 μM β-mercaptoethanol) on the antigen-coated filter plates at 37°C and 5% humidified CO_2 overnight, except for H5-specific plasmablasts which were incubated for 4 h. After washing with PBS, plates were incubated with 1% NP40 (Sigma) for 20 min at room temperature. Plates were washed with ELISA wash buffer and incubated sequentially with biotinylated anti-IgG (B7022, Sigma) and streptavidin-conjugated horseradish peroxidase (HRP; SA-5004, Vector Laboratories), each for 1 h at room temperature. After additional washes with PBS, substrate solution (5510-0050, SeraCare) was added. The reaction was quenched by washing with water. Spots were enumerated using a Biospot plate reader (Cellular Technology).

Bone marrow transplantation

Four-week-old CD137$^{-/-}$ mice were irradiated with 900 Rads and reconstituted via intravenous injection with 3×10^7 bone marrow cells isolated from the femur and tibia of WT (CD45.1) or CD137$^{-/-}$ mice (CD45.2). After 8 weeks, immune cell reconstitution was confirmed by flow cytometry.

QUANTIFICATION AND STATISTICAL ANALYSIS

All data were analyzed with Prism 8.2.0 software (GraphPad Prism). Statistical significance was assigned when $p < 0.05$. In each experiment in the Figure legends, the number of animals is indicated in scatterplot form with a symbol representing an individual animal. Additionally, the particular statistical test and number of independent experiments are indicated in the Figure legends. For immune cell analyses, data were analyzed by the Mann-Whitney test or Kruskal-Wallis ANOVA with Dunn's post-test. A Mann-Whitney test in lieu of an unpaired t test was used throughout for consistency, as some data had points at the level of detection. For serum antibody titer analyses, data were analyzed by two-way ANOVA with Sidak post-test. Bars indicate median values. No formal analytical method was used to determine whether the data met assumptions of the statistical approach.